

# Finite strain viscoplasticity with nonlinear kinematic hardening: phenomenological modeling and time integration

A.V. Shutov\*, R. Kreißig

*Institute of Mechanics, Chemnitz University of Technology, Str. d. Nationen 62,  
D-09111 Chemnitz, Germany*

---

## Abstract

This article deals with a viscoplastic material model of overstress type. The model is based on a multiplicative decomposition of the deformation gradient into elastic and inelastic part. An additional multiplicative decomposition of inelastic part is used to describe a nonlinear kinematic hardening of Armstrong-Frederick type.

Two implicit time-stepping methods are adopted for numerical integration of evolution equations, such that the plastic incompressibility constraint is exactly satisfied. The first method is based on the tensor exponential. The second method is a modified Euler-Backward method. Special numerical tests show that both approaches yield similar results even for finite inelastic increments.

The basic features of the material response, predicted by the material model, are illustrated with a series of numerical simulations.

*Key words:* Viscoplasticity, finite strains, kinematic hardening, inelastic incompressibility, integration algorithm, material testing.

---

*AMS Subject Classification:* 74C20; 74S05.

## Notation

$\mathbf{F}$	deformation gradient
$\mathbf{F}_i$	inelastic part of the deformation gradient
$\hat{\mathbf{F}}_e$	elastic part of the deformation gradient

---

\* Corresponding author. Tel.: +49-0-371-531-35024; fax: +49-0-371-531-23419.  
*Email address:* alexey.shutov@mb.tu-chemnitz.de (A.V. Shutov).

$\mathbf{F}_{ii}$	dissipative part of $\mathbf{F}_i$
$\tilde{\mathbf{F}}_{ie}$	energy storage part of $\mathbf{F}_i$
$\mathcal{K}$	current configuration
$\tilde{\mathcal{K}}$	reference configuration
$\hat{\mathcal{K}}$	stress-free intermediate configuration
$\check{\mathcal{K}}$	intermediate configuration of microstructure
$\mathbf{C}$	right Cauchy-Green tensor (see (6))
$\mathbf{C}_i$	inelastic right Cauchy-Green tensor (see (7) <sub>1</sub> )
$\mathbf{C}_{ii}$	inelastic right Cauchy-Green tensor of microstructure (see (7) <sub>2</sub> )
$\hat{\mathbf{C}}_e$	elastic right Cauchy-Green tensor (see (8) <sub>1</sub> )
$\check{\mathbf{C}}_{ie}$	elastic right Cauchy-Green tensor of microstructure (see (8) <sub>2</sub> )
$\mathbf{E}$	Green strain tensor (see (9) <sub>1</sub> )
$\mathbf{\Gamma}$	Almansi strain tensor (see (9) <sub>2</sub> )
$\mathbf{T}$	Cauchy stress tensor
$\mathbf{S}$	weighted Cauchy tensor (Kirchhoff tensor) (see (19))
$\hat{\mathbf{S}}, \tilde{\mathbf{T}}$	2nd Piola-Kirchhoff tensors operating on $\hat{\mathcal{K}}, \tilde{\mathcal{K}}$ , respectively (see (20))
$\tilde{\mathbf{X}}, \hat{\mathbf{X}}, \check{\mathbf{X}}$	backstress tensors operating on $\check{\mathcal{K}}, \hat{\mathcal{K}}$ and $\tilde{\mathcal{K}}$ , respectively (see (23))
$\hat{\Sigma}$	the driving force for inelastic flow (see (37) <sub>1</sub> )
$\check{\Sigma}$	the driving force for inelastic flow of microstructure (see (37) <sub>2</sub> )
$\mathbf{1}$	second-rank identity tensor
$\mathbf{M}^*, \mathbf{M}_*$	covariant pull-back and push-forward (see (4))
$(\mathbf{M}^{-T})^*, (\mathbf{M}^{-T})_*$	contravariant pull-back and push-forward (see (5))
$\mathbf{A} \cdot \mathbf{B} = \mathbf{AB}$	product (composition) of two second-rank tensors
$\mathbf{A} : \mathbf{B}$	scalar product of two second-rank tensors (see (22))
$\ \mathbf{A}\ $	$l_2$ norm of a second-rank tensor (Frobenius norm) (see (40) <sub>1</sub> )
$\ \mathbf{A}\ ^*$	induced norm of a second-rank tensor (spectral norm) (see (70))
$(\cdot)^D$	deviatoric part of a tensor (see (40) <sub>2</sub> )
$(\cdot)^T$	transposition of a tensor
$(\cdot)^{-T}$	inverse of transposed
$\text{tr}(\cdot)$	trace of a second-order tensor
$\overset{\Delta}{(\cdot)}$	covariant Oldroyd rate with respect to $\hat{\mathcal{K}}$ (see (15) <sub>1</sub> )
$\overset{\diamond}{(\cdot)}$	covariant Oldroyd rate with respect to $\check{\mathcal{K}}$ (see (15) <sub>2</sub> )
$\overline{(\cdot)}$	unimodular part of a tensor (see (28))
$\text{sym}(\cdot)$	symmetric part of a tensor (see (18))
$\text{skew}(\cdot)$	skew-symmetric part of a tensor (see (67) <sub>2</sub> )
$\langle x \rangle$	MacCauley bracket (see (41) <sub>3</sub> )
$\psi$	specific free energy
$\delta_i$	specific internal dissipation (see (31))
$K$	initial yield stress
$R$	isotropic hardening
${}^tR$	trial isotropic hardening (see (87) <sub>2</sub> )
$s$	inelastic arc length
$s_d$	dissipative part of $s$

$s_e$	energy storage part of $s$ (see (14))
$\lambda_i$	proportionality factor (inelastic multiplier) (see (41) <sub>1</sub> )
$f$	overstress (see (41) <sub>2</sub> )
$Sym$	space of symmetric second-rank tensors
$\mathfrak{F}$	norm of the driving force (see (53))
$\xi$	incremental inelastic parameter (see (78))
$\rho_R$	mass density in the reference configuration
$k$	bulk modulus (see (26))
$\mu$	shear modulus (see (26))
$c$	bulk modulus of microstructure (see (27) <sub>1</sub> )
$\gamma$	hardening modulus (see (27) <sub>2</sub> )
$\varepsilon$	technical strain (see (93) <sub>1</sub> )
$\phi$	shear strain (see (94) <sub>1</sub> )
$\sigma, \tau$	axial and shear stresses, respectively

## 1 Introduction

New materials, such as ultrafine-grained-aluminium (see the papers [15], [28]), are of special interest for many practical applications. To promote the innovation of the new materials, the robust numerical simulation of the material response is required. It is desirable to have a phenomenological description of the material which on the one hand takes important phenomena into account, and on the other hand enables stable numerical computations.

In this paper we investigate the simulation of rate-dependent material behavior with equilibrium hysteresis effect (for the general introduction to the theory of viscoplasticity see, for example, [33], [23], [12]).

The Bauschinger effect is observed in most metals under non-monotonic loading. The most popular approach to describe the Bauschinger effect was proposed by Armstrong and Frederick [2] in 1966. Application of the Armstrong-Frederick hardening concept within the framework of Perzyna type viscoplasticity (see [33]) yields the classical material model of overstress type (see [3], [23]). This model has the advantage that it admits simple rheological interpretation (see fig. 1.a). Such phenomena as creep, relaxation and nonlinear kinematic hardening are taken into account by the model. Simple modification of this model is possible to include isotropic hardening as well <sup>1</sup>.

Several strategies can be adopted for the generalization of this model to finite strains (see,

---

<sup>1</sup> The diagram in fig. 1.a provides insight into the rheological modeling of kinematic hardening. To the best of our knowledge, there is no simple rheological diagram of viscoplastic material with isotropic hardening.

for example, [6], [38], [26], [37], [24], [13], [31]). Some of the generalizations were analyzed numerically in [5]. Following the elegant approach of Lion [24], we use the rheological interpretation (fig. 1.a) of the classical model to construct its finite-strain counterpart.

The specific assumptions of the material modeling used in this paper are as follows:

- Multiplicative decomposition of the deformation gradient into elastic and inelastic part:  $\mathbf{F} = \check{\mathbf{F}}_e \mathbf{F}_i$  ([21], [22]).
- Multiplicative decomposition of the inelastic part into energy storage part and dissipative part:  $\mathbf{F}_i = \check{\mathbf{F}}_{ie} \mathbf{F}_{ii}$  ([24]).
- Free energy is a sum of appropriate isotropic strain energy functions ([24]).

The resulting material model takes both kinematic and isotropic hardening into account. The thermodynamic consistency is proved.

The purpose of the present paper is threefold. First, we formulate the material model under consideration. In particular, we transform the constitutive equations to the reference configuration in order to simplify the numerical treatment. Next, two implicit schemes for the numerical integration of evolution equations are developed. Finally, we analyse numerically the basic properties of the material response, predicted by the model.

A global *implicit* time stepping procedure in the context of displacement based FEM requires a proper stress algorithm (local integration algorithm) [40]. Such algorithm provides the stresses and the consistent tangent operator as a function of the strain history locally at each integration point. A set of internal variables is used in this paper to describe the history dependence, and the stress algorithm includes *implicit* integration of a system of differential (evolution) and algebraic equations.

Two most popular implicit schemes for integration of inelastic strains in the context of viscoplasticity/plasticity are:

- *Backward-Euler scheme*, also referred as *implicit Euler scheme* (see, for example, [10], [35], [36], [13], [5]).
- *Exponential scheme*, also referred as *Euler scheme with exponential map* (see, for example, [39], [29], [30], [5]).

The exponential scheme is advantageous since it retains the inelastic incompressibility even for finite time steps. Thus, an important geometric property of the solution is automatically preserved. Moreover, the numerical error of Euler-Backward method, related to the violation of incompressibility, *tends to accumulate over time* (see, for example, [5], [14]). Therefore, even for small time steps, the numerical solution deviates from the exact solution after some period of time.

Helm [14] modified the classical Euler-Backward scheme, using a projection on the group of unimodular tensors, to enforce the incompressibility of inelastic flow.

In this work we implement in a uniform manner both modified Euler-Backward method (MEBM) and the exponential method (EM). Both methods result in a nonlinear system of equations with respect to strain-like internal variables  $\mathbf{C}_i = \mathbf{F}_i^T \mathbf{F}_i$ ,  $\mathbf{C}_{ii} = \mathbf{F}_{ii}^T \mathbf{F}_{ii}$  and  $\xi = \lambda_i \Delta t$ <sup>2</sup>. This nonlinear system is split into two subproblems:

First subproblem: Finding  $\mathbf{C}_i, \mathbf{C}_{ii}$  with a given  $\xi$ .

Second subproblem: Finding  $\xi$ , such that an incremental consistency condition is satisfied. This adapted strategy is more robust than the straightforward application of a nonlinear solver to the original system of equations. At the same time, this approach is not limited by the special form of the free energy, and finite elastic strains are likewise allowed. Moreover, the stress algorithms are applicable in the limiting case of rate-independent plasticity (as viscosity tends to zero).

Although the material response is anisotropic, it is shown that MEBM as well as EM *exactly preserve the symmetry* of  $\mathbf{C}_i$  and  $\mathbf{C}_{ii}$ . Furthermore, the accuracy of both integration algorithms is verified with the help of special numerical tests. Both methods provide similar results with almost the same integration error. A common feature of MEBM and EM is that the numerical error is not accumulated over time.

The phenomenological description of each specific material can be schematically subdivided into three steps:

- Material testing, such that the important phenomena make themselves evident.
- Choosing an appropriate phenomenological model, that reproduces qualitatively the experimental data.
- Parameter identification, using the experimental data.

To illustrate the basic characteristics of the material model we simulate a series of material testing experiments. These experiments are uniaxial tension and torsion under monotonic and cyclic loading. In particular, we conclude that the material model can be used (after a proper parameter identification) to describe the mechanical response of an aluminium alloy processed by ECA-pressing [15], [28].

Throughout this article, bold-faced symbols denote first- and second-rank tensors in  $\mathbb{R}^3$ . Expression  $a := b$  means  $a$  is defined to be another name for  $b$ .

## 2 Material model of finite viscoplasticity

The material model is motivated by the rheological diagram in fig. 1.a. This diagram takes the kinematic hardening of Armstrong-Frederick type into account (for the sake of simplicity the isotropic hardening is omitted in the diagram). The total inelastic strains and the inelastic strains of microstructure are used as internal variables. The evolution of these quantities is closely related to the energy dissipation during the inelastic processes.

---

<sup>2</sup>  $\xi \geq 0$  is an incremental inelastic parameter, defined by (78)

Besides, additional real-valued strain-like internal variables are introduced in order to describe a nonlinear isotropic hardening.

## 2.1 Kinematics

For a fixed time instant  $t \geq 0$  let  $\mathcal{K} \subset \mathbb{R}^3$  be a current configuration occupied by the solid. Suppose  $\tilde{\mathcal{K}} \subset \mathbb{R}^3$  is the reference configuration, which uniquely designates the material points. Let us consider the motion law in the form  $\chi_t : \tilde{\mathcal{K}} \rightarrow \mathcal{K}$ . For every point  $\mathbf{P} \in \tilde{\mathcal{K}}$  we define the deformation gradient tensor  $\mathbf{F} := \frac{\partial \chi_t(\mathbf{P})}{\partial \mathbf{P}}$ . The deformation gradient  $\mathbf{F}$  transforms a material line element  $d\mathbf{X}$  on the reference configuration  $\tilde{\mathcal{K}}$  into a current material line element  $d\mathbf{x}$

$$d\mathbf{x} = \mathbf{F} d\mathbf{X}. \quad (1)$$

Let us consider the classical multiplicative decomposition of the deformation gradient  $\mathbf{F}$  into *elastic part*  $\hat{\mathbf{F}}_e$  and *inelastic part*  $\mathbf{F}_i$  ([21], [22])

$$\mathbf{F} = \hat{\mathbf{F}}_e \mathbf{F}_i. \quad (2)$$

The mechanical justification uses the idea of the local (within a neighborhood of the material point) elastic unloading. The transformation rule (1) is represented as a combination of two linear operators

$$d\mathbf{x} = \hat{\mathbf{F}}_e (\mathbf{F}_i d\mathbf{X}).$$

Therefore, we can interpret  $\mathbf{F}_i d\mathbf{X}$  as a fictitious material line element on some intermediate configuration  $\hat{\mathcal{K}}$  (see fig. 1.b). We will call this configuration the *stress-free intermediate configuration*.

A second multiplicative decomposition is introduced in order to simulate a nonlinear kinematic hardening of Armstrong-Frederick type. Following Lion [24], we decompose the inelastic part  $\mathbf{F}_i$  into *energy storage part*  $\check{\mathbf{F}}_{ie}$  and *dissipative part*  $\mathbf{F}_{ii}$

$$\mathbf{F}_i = \check{\mathbf{F}}_{ie} \mathbf{F}_{ii}. \quad (3)$$

The energy storage part  $\check{\mathbf{F}}_{ie}$  describes the heterogeneity of elastic strains associated with the energy storage on the microscale. The dissipative part  $\mathbf{F}_{ii}$  can be attributed to slip processes on the microscale (see [24], [13] for details). Decomposition (3) implements the *intermediate configuration of microstructure*<sup>3</sup>  $\check{\mathcal{K}}$  (see fig. 1.b). The commutative diagram in fig. 1.b summarizes both multiplicative decompositions.

In this paper we deal with second-order tensors, which operate on configurations  $\mathcal{K}$ ,  $\tilde{\mathcal{K}}$ ,  $\hat{\mathcal{K}}$ ,  $\check{\mathcal{K}}$ . Pull-back (push-forward) operations describe the transformation of tensor fields during the change of configurations. Let  $\mathbf{M} \in \{\mathbf{F}, \mathbf{F}_i, \mathbf{F}_{ii}, \hat{\mathbf{F}}_e, \check{\mathbf{F}}_{ie}\}$  be a linear transformation of

<sup>3</sup> In [24] the similar configuration is called the *intermediate configuration of kinematic hardening*.

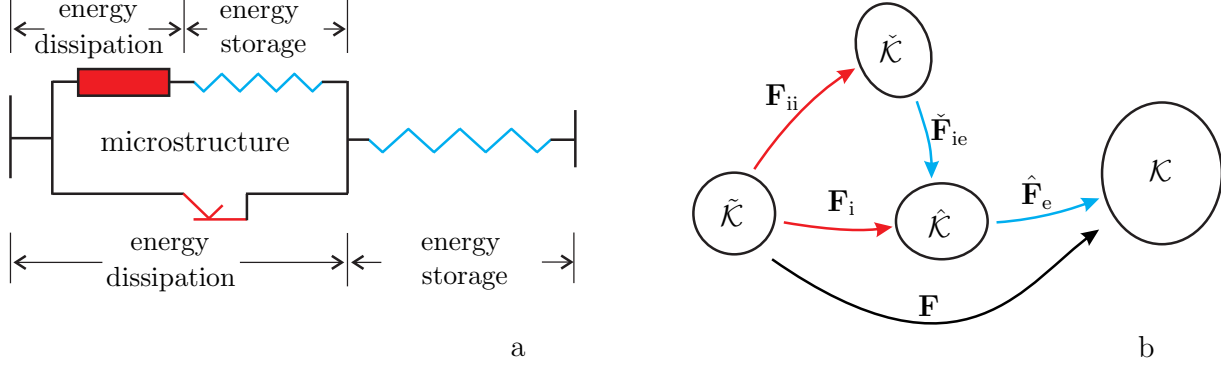


Fig. 1. Rheological model (a) and a commutative diagram (b) showing corresponding configurations with transformations of material line elements.

material line elements on two different configurations. We define corresponding *pull-back* and *push-forward of covariant tensor field* by

$$\mathbf{M}^*(\cdot) := \mathbf{M}^T(\cdot)\mathbf{M}, \quad \mathbf{M}_*(\cdot) := \mathbf{M}^{-T}(\cdot)\mathbf{M}^{-1}. \quad (4)$$

*Pull-back and push-forward of contravariant tensor field* are given by

$$(\mathbf{M}^{-T})^*(\cdot) = \mathbf{M}^{-1}(\cdot)\mathbf{M}^{-T}, \quad (\mathbf{M}^{-T})_*(\cdot) = \mathbf{M}(\cdot)\mathbf{M}^T. \quad (5)$$

Thus, the right Cauchy-Green tensor is a covariant pull-back of  $\mathbf{1}$

$$\mathbf{C} := \mathbf{F}^*\mathbf{1} = \mathbf{F}^T\mathbf{F}. \quad (6)$$

In the same manner, we define the inelastic right Cauchy-Green tensor  $\mathbf{C}_i$  and inelastic right Cauchy-Green tensor  $\mathbf{C}_{ii}$  of microstructure:

$$\mathbf{C}_i := \mathbf{F}_i^*\mathbf{1} = \mathbf{F}_i^T\mathbf{F}_i, \quad \mathbf{C}_{ii} := \mathbf{F}_{ii}^*\mathbf{1} = \mathbf{F}_{ii}^T\mathbf{F}_{ii}. \quad (7)$$

Further, the elastic right Cauchy-Green tensor  $\hat{\mathbf{C}}_e$  and the elastic right Cauchy-Green tensor  $\check{\mathbf{C}}_{ie}$  of microstructure are defined by

$$\hat{\mathbf{C}}_e := \hat{\mathbf{F}}_e^*\mathbf{1} = \hat{\mathbf{F}}_e^T\hat{\mathbf{F}}_e, \quad \check{\mathbf{C}}_{ie} := \check{\mathbf{F}}_{ie}^*\mathbf{1} = \check{\mathbf{F}}_{ie}^T\check{\mathbf{F}}_{ie}. \quad (8)$$

The tensors

$$\mathbf{E} := \frac{1}{2}(\mathbf{C} - \mathbf{1}), \quad \mathbf{\Gamma} := \mathbf{F}_*\mathbf{E} = \mathbf{F}^{-T}\mathbf{E}\mathbf{F}^{-1} \quad (9)$$

are termed the Green strain tensor and the Almansi strain tensor, respectively. Basing on  $\mathbf{E}$ , we define a corresponding strain tensor  $\hat{\mathbf{\Gamma}}$ , which operates on  $\hat{\mathcal{K}}$

$$\hat{\mathbf{\Gamma}} := (\mathbf{F}_i)_*\mathbf{E} = \mathbf{F}_i^{-T}\mathbf{E}\mathbf{F}_i^{-1}.$$

Multiplicative decomposition (2) implements the additive decomposition of  $\hat{\mathbf{\Gamma}}$ :

$$\mathbf{F} = \hat{\mathbf{F}}_e\mathbf{F}_i \quad \Rightarrow \quad \hat{\mathbf{\Gamma}} = \hat{\mathbf{\Gamma}}_i + \hat{\mathbf{\Gamma}}_e, \quad (10)$$

where  $\hat{\mathbf{\Gamma}}_i$  is a purely inelastic Almansi tensor

$$\hat{\mathbf{\Gamma}}_i := \frac{1}{2}(\mathbf{1} - \mathbf{F}_i^{-T}\mathbf{F}_i^{-1})$$

and  $\hat{\mathbf{\Gamma}}_e$  is the elastic Green tensor

$$\hat{\mathbf{\Gamma}}_e := \frac{1}{2}(\hat{\mathbf{F}}_e^T\hat{\mathbf{F}}_e - \mathbf{1}) = \frac{1}{2}(\hat{\mathbf{C}}_e - \mathbf{1}). \quad (11)$$

Analogously, multiplicative decomposition (3) implements the additive decomposition of the pull-back of the inelastic Almansi tensor  $\hat{\mathbf{\Gamma}}_i$  to  $\check{\mathcal{K}}$ :

$$\check{\mathbf{\Gamma}}_i := \check{\mathbf{F}}_{ie}^*\hat{\mathbf{\Gamma}}_i = \check{\mathbf{F}}_{ie}^T\hat{\mathbf{\Gamma}}_i\check{\mathbf{F}}_{ie},$$

$$\mathbf{F}_i = \check{\mathbf{F}}_{ie}\mathbf{F}_{ii} \quad \Rightarrow \quad \check{\mathbf{\Gamma}}_i = \check{\mathbf{\Gamma}}_{ii} + \check{\mathbf{\Gamma}}_{ie}, \quad (12)$$

where

$$\check{\mathbf{\Gamma}}_{ii} := \frac{1}{2}(\mathbf{1} - \mathbf{F}_{ii}^{-T}\mathbf{F}_{ii}^{-1}), \quad \check{\mathbf{\Gamma}}_{ie} := \frac{1}{2}(\check{\mathbf{F}}_{ie}^T\check{\mathbf{F}}_{ie} - \mathbf{1}) = \frac{1}{2}(\check{\mathbf{C}}_{ie} - \mathbf{1}). \quad (13)$$

Finally, we define the inelastic pull-back of  $\hat{\mathbf{\Gamma}}_i$  to  $\tilde{\mathcal{K}}$

$$\tilde{\mathbf{\Gamma}}_i := \mathbf{F}_i^*\hat{\mathbf{\Gamma}}_i.$$

In this paper, the evolution of isotropic hardening is taken into account, similar to the Armstrong-Frederick rule. To this end, we introduce two real-valued internal variables of strain type:  $s$  and  $s_d$ . The first variable is the classical inelastic arc length, and  $s_d$  is interpreted as a dissipative part of  $s$ , such that

$$s_e := s - s_d \quad (14)$$

controls the energy stored due to the isotropic hardening (see section 2.3).

## 2.2 The concept of dual variables

The formalism of dual variables developed by Haupt and Tsakmakis [11] specifies the choice of stress and strain variables as well as their time derivatives. According to this concept, we introduce the covariant Oldroyd rates  $\overset{\Delta}{(\cdot)}$ ,  $\overset{\diamond}{(\cdot)}$  with respect to the stress-free configuration  $\hat{\mathcal{K}}$  and the microstructural configuration  $\check{\mathcal{K}}$ , respectively,

$$\overset{\Delta}{(\cdot)} := \mathbf{F}_{i*} \left( \left( \mathbf{F}_i^*(\cdot) \right) \dot{\phantom{\cdot}} \right), \quad \overset{\diamond}{(\cdot)} := \mathbf{F}_{ii*} \left( \left( \mathbf{F}_{ii}^*(\cdot) \right) \dot{\phantom{\cdot}} \right), \quad (15)$$



where  $(\cdot)^\cdot$  stands for material time derivative. The alternative representation of covariant Oldroyd derivatives is as follows

$$\overset{\Delta}{(\cdot)} = (\cdot)^\cdot + \hat{\mathbf{L}}_i^T(\cdot) + (\cdot)\hat{\mathbf{L}}_i, \quad \overset{\diamond}{(\cdot)} = (\cdot)^\cdot + \check{\mathbf{L}}_{ii}^T(\cdot) + (\cdot)\check{\mathbf{L}}_{ii}, \quad (16)$$

$$\hat{\mathbf{L}}_i := \dot{\mathbf{F}}_i \mathbf{F}_i^{-1}, \quad \check{\mathbf{L}}_{ii} := \dot{\mathbf{F}}_{ii} \mathbf{F}_{ii}^{-1}.$$

Equation (15) yields the inelastic deformation rates  $\overset{\Delta}{\hat{\Gamma}}_i$  and  $\overset{\diamond}{\check{\Gamma}}_{ii}$  as symmetric parts of  $\hat{\mathbf{L}}_i$  and  $\check{\mathbf{L}}_{ii}$ , respectively:

$$\overset{\Delta}{\hat{\Gamma}}_i = \text{sym}(\hat{\mathbf{L}}_i), \quad \overset{\diamond}{\check{\Gamma}}_{ii} = \text{sym}(\check{\mathbf{L}}_{ii}), \quad (17)$$

where the symmetric part of a tensor is given by

$$\text{sym}(\cdot) := \frac{1}{2} \left( (\cdot) + (\cdot)^T \right). \quad (18)$$

Let  $\mathbf{T}$  be the Cauchy stress tensor. The weighted Cauchy tensor (or Kirchhoff stress tensor) is defined by

$$\mathbf{S} := (\det \mathbf{F}) \mathbf{T}. \quad (19)$$

Now, we define the 2nd Piola-Kirchhoff tensors operating on  $\hat{\mathcal{K}}$  and  $\check{\mathcal{K}}$  using a contravariant pull-back of  $\mathbf{S}$

$$\hat{\mathbf{S}} := (\hat{\mathbf{F}}_e^{-T})^* \mathbf{S}, \quad \tilde{\mathbf{T}} := (\mathbf{F}^{-T})^* \mathbf{S} = (\mathbf{F}_i^{-T})^* \hat{\mathbf{S}}. \quad (20)$$

The introduced stress and strain tensors form the following conjugate pairs:  $(\mathbf{S}, \boldsymbol{\Gamma})$ ,  $(\hat{\mathbf{S}}, \hat{\boldsymbol{\Gamma}})$ ,  $(\tilde{\mathbf{T}}, \mathbf{E})$ , such that the work and the stress power are invariant under the change of configuration:

$$\mathbf{S} : \boldsymbol{\Gamma} = \hat{\mathbf{S}} : \hat{\boldsymbol{\Gamma}} = \tilde{\mathbf{T}} : \mathbf{E}, \quad \hat{\mathbf{S}} : \overset{\Delta}{\hat{\boldsymbol{\Gamma}}} = \tilde{\mathbf{T}} : \dot{\mathbf{E}}. \quad (21)$$

Here " : " denotes the scalar product of two second-rank tensors

$$\mathbf{A} : \mathbf{B} := \text{tr}(\mathbf{A} \cdot \mathbf{B}^T). \quad (22)$$

Next, we denote by  $\check{\mathbf{X}}$  the backstress tensor, which operates on the intermediate configuration  $\check{\mathcal{K}}$  of microstructure. This tensor can be interpreted as a generalized force, associated with strain measure  $\check{\boldsymbol{\Gamma}}_i$  and strain rate  $\overset{\diamond}{\check{\boldsymbol{\Gamma}}}_i$ . According to the concept of dual variables, we define transformation rules for the backstress tensor, such that quantities  $\check{\mathbf{X}} : \check{\boldsymbol{\Gamma}}_i$  and  $\check{\mathbf{X}} : \overset{\diamond}{\check{\boldsymbol{\Gamma}}}_i$  remain invariant under the change of configuration:

$$\check{\mathbf{X}} := (\mathbf{F}_{ii}^{-T})^* \check{\mathbf{X}} = \mathbf{F}_{ii}^{-1} \check{\mathbf{X}} \mathbf{F}_{ii}^{-T}, \quad \hat{\mathbf{X}} := (\check{\mathbf{F}}_{ie}^{-T})_* \check{\mathbf{X}} = \check{\mathbf{F}}_{ie} \check{\mathbf{X}} \check{\mathbf{F}}_{ie}^T, \quad (23)$$

$$\check{\mathbf{X}} : \check{\boldsymbol{\Gamma}}_i = \hat{\mathbf{X}} : \hat{\boldsymbol{\Gamma}}_i = \tilde{\mathbf{X}} : \tilde{\boldsymbol{\Gamma}}_i, \quad \check{\mathbf{X}} : \overset{\diamond}{\check{\boldsymbol{\Gamma}}}_i = \hat{\mathbf{X}} : \overset{\Delta}{\hat{\boldsymbol{\Gamma}}}_i = \tilde{\mathbf{X}} : \dot{\tilde{\boldsymbol{\Gamma}}}_i. \quad (24)$$

### 2.3 Free energy

Suppose that the free energy is given as a sum of isotropic functions<sup>4</sup> (cf. [24], [13])

$$\psi = \psi(\hat{\mathbf{T}}_e, \check{\mathbf{T}}_{ie}, s_e) = \psi_{el}(\hat{\mathbf{T}}_e) + \psi_{kin}(\check{\mathbf{T}}_{ie}) + \psi_{iso}(s_e), \quad (25)$$

where the tensors  $\hat{\mathbf{T}}_e$  and  $\check{\mathbf{T}}_{ie}$  are defined by (11), (13)<sub>2</sub>. Here,  $\psi_{el}(\hat{\mathbf{T}}_e)$  corresponds to the energy, stored due to macroscopic elastic deformations. The "inelastic" part  $\psi_{kin}(\check{\mathbf{T}}_{ie}) + \psi_{iso}(s_e)$  represents the energy, stored in the microstructure during the viscoplastic flow due to the heterogeneity of dislocations. The following special form of the free energy can be used

$$\rho_R \psi_{el}(\hat{\mathbf{T}}_e) = \frac{k}{2} (\ln \sqrt{\det \hat{\mathbf{C}}_e})^2 + \frac{\mu}{2} (\text{tr} \hat{\mathbf{C}}_e - 3), \quad (26)$$

$$\rho_R \psi_{kin}(\check{\mathbf{T}}_{ie}) = \frac{c}{4} (\text{tr} \check{\mathbf{C}}_{ie} - 3), \quad \rho_R \psi_{iso}(s_e) = \frac{\gamma}{2} (s_e)^2. \quad (27)$$

Here,  $k > 0$ ,  $\mu > 0$ ,  $c \geq 0$ ,  $\gamma \geq 0$  are material constants. The overline  $\overline{(\cdot)}$  denotes the unimodular part of a tensor

$$\overline{\mathbf{A}} := (\det \mathbf{A})^{-1/3} \mathbf{A}. \quad (28)$$

Denote by  $\frac{\partial \alpha(\mathbf{A})}{\partial \mathbf{A}}$  the derivative of real-valued function  $\alpha$  with respect to tensor-valued argument  $\mathbf{A}$  such that

$$\delta \alpha = \frac{\partial \alpha(\mathbf{A})}{\partial \mathbf{A}} : \delta \mathbf{A}. \quad (29)$$

Using this notation, we introduce formally the following potential relations for stresses  $\hat{\mathbf{S}}$ ,  $\check{\mathbf{X}}$  and for isotropic hardening  $R$

$$\hat{\mathbf{S}} = \rho_R \frac{\partial \psi_{el}(\hat{\mathbf{T}}_e)}{\partial \hat{\mathbf{T}}_e}, \quad \check{\mathbf{X}} = \rho_R \frac{\partial \psi_{kin}(\check{\mathbf{T}}_{ie})}{\partial \check{\mathbf{T}}_{ie}}, \quad R = \rho_R \frac{\partial \psi_{iso}(s_e)}{\partial s_e}. \quad (30)$$

### 2.4 Clausius-Duhem inequality

The Clausius-Duhem inequality imposes an additional constraint on the material response, which states that the internal dissipation is always nonnegative. For isothermal processes the specific internal dissipation  $\delta_i$  takes the form (see [12])

$$\delta_i := \frac{1}{\rho_R} \tilde{\mathbf{T}} : \dot{\mathbf{E}} - \dot{\psi} \geq 0. \quad (31)$$

Now, let us rewrite this expression, using relations of previous subsections. First, we note that  $\hat{\mathbf{S}}$  and  $\check{\mathbf{X}}$  are isotropic functions of  $\hat{\mathbf{T}}_e$  and  $\check{\mathbf{T}}_{ie}$ , respectively. In particular, since  $\hat{\mathbf{S}}$  and

<sup>4</sup> the first two terms of this additive split can be motivated by the rheological model (fig. 1.a).

$\hat{\Gamma}_e$  commute, we get

$$\hat{\mathbf{S}} : \left( \hat{\mathbf{L}}_i^T \hat{\Gamma}_e + \hat{\Gamma}_e \hat{\mathbf{L}}_i \right) \stackrel{(22)}{=} 2 \left( \hat{\Gamma}_e \hat{\mathbf{S}} \right) : \hat{\mathbf{L}}_i \stackrel{(17)_1}{=} 2 \left( \hat{\Gamma}_e \hat{\mathbf{S}} \right) : \hat{\Gamma}_i. \quad (32)$$

Further, note that

$$\hat{\mathbf{S}} : \hat{\Gamma} \stackrel{(10)}{=} \hat{\mathbf{S}} : \hat{\Gamma}_e + \hat{\mathbf{S}} : \hat{\Gamma}_i \stackrel{(16)_1}{=} \hat{\mathbf{S}} : \dot{\Gamma}_e + \hat{\mathbf{S}} : \left( \hat{\mathbf{L}}_i^T \hat{\Gamma}_e + \hat{\Gamma}_e \hat{\mathbf{L}}_i \right) + \hat{\mathbf{S}} : \hat{\Gamma}_i \stackrel{(32)}{=} \hat{\mathbf{S}} : \dot{\Gamma}_e + \left( \hat{\mathbf{C}}_e \hat{\mathbf{S}} \right) : \hat{\Gamma}_i. \quad (33)$$

In the same way, since  $\check{\mathbf{X}}$  and  $\check{\Gamma}_{ie}$  commute, we obtain from (12), (16)<sub>2</sub>, (17)<sub>2</sub>

$$\check{\mathbf{X}} : \check{\Gamma}_i = \check{\mathbf{X}} : \dot{\Gamma}_{ie} + \left( \check{\mathbf{C}}_{ie} \check{\mathbf{X}} \right) : \check{\Gamma}_{ii}. \quad (34)$$

Thus, we get for the stress power

$$\begin{aligned} \hat{\mathbf{S}} : \hat{\Gamma} &\stackrel{(24)}{=} \hat{\mathbf{S}} : \hat{\Gamma} - \check{\mathbf{X}} : \hat{\Gamma}_i + \check{\mathbf{X}} : \check{\Gamma}_i \\ &\stackrel{(33),(34)}{=} \hat{\mathbf{S}} : \dot{\Gamma}_e + \left( \hat{\mathbf{C}}_e \hat{\mathbf{S}} - \check{\mathbf{X}} \right) : \hat{\Gamma}_i + \check{\mathbf{X}} : \dot{\Gamma}_{ie} + \left( \check{\mathbf{C}}_{ie} \check{\mathbf{X}} \right) : \check{\Gamma}_{ii}. \end{aligned} \quad (35)$$

Hence, the internal dissipation takes the form

$$\begin{aligned} \delta_i &= \frac{1}{\rho_R} \tilde{\mathbf{T}} : \dot{\mathbf{E}} - \dot{\psi} \stackrel{(21)_2}{=} \frac{1}{\rho_R} \hat{\mathbf{S}} : \hat{\Gamma} - \dot{\psi} \stackrel{(35)}{=} \left( \frac{1}{\rho_R} \hat{\mathbf{S}} - \frac{\partial \psi_{el}}{\partial \hat{\Gamma}_e} \right) : \dot{\Gamma}_e + \left( \frac{1}{\rho_R} \check{\mathbf{X}} - \frac{\partial \psi_{kin}}{\partial \check{\Gamma}_{ie}} \right) : \dot{\Gamma}_{ie} \\ &\quad + \frac{1}{\rho_R} \left( \hat{\mathbf{C}}_e \hat{\mathbf{S}} - \check{\mathbf{X}} \right) : \hat{\Gamma}_i + \frac{1}{\rho_R} \left( \check{\mathbf{C}}_{ie} \check{\mathbf{X}} \right) : \check{\Gamma}_{ii} - \frac{\partial \psi_{iso}}{\partial s_e} \dot{s}_e. \end{aligned} \quad (36)$$

We abbreviate

$$\hat{\Sigma} := \hat{\mathbf{C}}_e \hat{\mathbf{S}} - \check{\mathbf{X}}, \quad \check{\Xi} := \check{\mathbf{C}}_{ie} \check{\mathbf{X}}. \quad (37)$$

Finally, taking into account potential relations (30) and definition (14), we simplify (36) to obtain the Clausius-Duhem inequality in the form

$$\rho_R \delta_i = \left( \hat{\Sigma} : \hat{\Gamma}_i - R \dot{s} \right) + \check{\Xi} : \check{\Gamma}_{ii} + R \dot{s}_d \geq 0. \quad (38)$$

## 2.5 Evolution equations

Following the standard procedure, we formulate the evolution equations for internal variables so that inequality (38) holds for arbitrary mechanical loadings (cf. [24], [13]).

$$\hat{\Gamma}_i := \lambda_i \frac{\hat{\Sigma}^D}{\|\hat{\Sigma}^D\|}, \quad \check{\Gamma}_{ii} := \lambda_i \check{\Xi}^D, \quad (39)$$

$$\begin{aligned}\dot{s} &:= \sqrt{\frac{2}{3}}\lambda_i, & \dot{s}_d &:= \frac{\beta}{\gamma}\dot{s}R, \\ \|\mathbf{A}\| &:= \sqrt{\mathbf{A} : \mathbf{A}}, & \mathbf{A}^D &:= \mathbf{A} - \frac{1}{3}\text{tr}(\mathbf{A})\mathbf{1},\end{aligned}\tag{40}$$

where the inelastic multiplier  $\lambda_i$  is determined according to the Perzyna rule [32]

$$\lambda_i := \frac{1}{\eta} \left\langle \frac{1}{k_0} f \right\rangle^m, \quad f := \|\hat{\Sigma}^D\| - \sqrt{\frac{2}{3}}[K + R], \quad \langle x \rangle := \max(x, 0).\tag{41}$$

Here,  $\varkappa \geq 0$ ,  $\eta \geq 0$ ,  $m \geq 1$ ,  $\beta \geq 0$ ,  $K > 0$  are material parameters,  $k_0 > 0$  is used to get a dimensionless term in the bracket.

Let us show that inequality (38) is fulfilled. For instance, we prove that the parenthetical term in (38) is nonnegative. Indeed,

$$\left( \hat{\Sigma} : \hat{\Gamma}_i - R \dot{s} \right) = \lambda_i \left( \|\hat{\Sigma}^D\| - \sqrt{\frac{2}{3}}R \right) = \begin{cases} 0 & \text{if } f < 0 \ (\lambda_i = 0) \\ \lambda_i(f + \sqrt{\frac{2}{3}}K) & \text{if } f > 0 \ (\lambda_i > 0) \end{cases}.$$

Therefore, the material model, defined in sections 2.3 and 2.5, is *thermodynamically consistent*.

According to the evolution equations (39), the tensors  $\hat{\Sigma}^D$  and  $\check{\Xi}^D$  are termed *the driving force for inelastic flow* and *the driving force for inelastic flow of microstructure*, respectively. Note that both flows are incompressible. In fact,

$$(\det \mathbf{F}_i)' = (\det \mathbf{F}_i) \text{tr} \left( \hat{\Gamma}_i \right) = 0, \quad (\det \mathbf{F}_{ii})' = (\det \mathbf{F}_{ii}) \text{tr} \left( \check{\Gamma}_{ii} \right) = 0.\tag{42}$$

Under appropriate initial conditions, it follows from (42) that

$$\det \mathbf{F}_i = \det \mathbf{F}_{ii} = \det \mathbf{C}_i = \det \mathbf{C}_{ii} = 1.\tag{43}$$

The inelastic flow takes place if the overstress  $f$  is positive. A case of rate-independent plasticity is covered by these evolution equations as viscosity  $\eta$  tends to zero.

## 2.6 Transformation to the reference configuration

A direct numerical treatment of Oldroyd derivatives in (39), formulated with respect to fictitious configurations  $\hat{\mathcal{K}}$  and  $\check{\mathcal{K}}$ , is complicated. In this subsection we rewrite the material model in terms of strain-like internal variables  $\mathbf{C}_i$ ,  $\mathbf{C}_{ii}$ ,  $s$ ,  $s_d$  such that the rate of  $\mathbf{C}_i$ ,  $\mathbf{C}_{ii}$  will be given by the material time derivatives  $\dot{\mathbf{C}}_i$ ,  $\dot{\mathbf{C}}_{ii}$ . The transformation of the model includes:

- representation of the free energy  $\psi$  through  $\mathbf{C}$ ,  $\mathbf{C}_i$ ,  $\mathbf{C}_{ii}$ ,  $s$ ,  $s_d$ .

- transformation of the potential relations for stresses.
- representation of  $\|\hat{\Sigma}^D\|$  through  $\mathbf{C}, \mathbf{C}_i, \mathbf{C}_{ii}$ .
- transformation of the evolution equations.

### 2.6.1 Representation of the free energy

Let  $(J_1, J_2, J_3)$  be a full system of invariants of a second-rank tensor, defined by

$$J_1(\mathbf{A}) := \text{tr } \mathbf{A}, \quad J_2(\mathbf{A}) := \frac{1}{2} \text{tr } \mathbf{A}^2, \quad J_3(\mathbf{A}) := \frac{1}{3} \text{tr } \mathbf{A}^3.$$

Then, using multiplicative decompositions (2), (3) and the property  $\text{tr}(\mathbf{AB}) = \text{tr}(\mathbf{BA})$ , it is easily proved that

$$J_k(\hat{\mathbf{C}}_e) = J_k(\mathbf{C}\mathbf{C}_i^{-1}), \quad J_k(\check{\mathbf{C}}_{ie}) = J_k(\mathbf{C}_i\mathbf{C}_{ii}^{-1}), \quad k = 1, 2, 3. \quad (44)$$

Since  $\psi_{\text{el}}$  and  $\psi_{\text{kin}}$  are isotropic functions, it follows from (25), (44) that

$$\psi = \psi(\mathbf{C}, \mathbf{C}_i, \mathbf{C}_{ii}, s, s_d) = \psi_{\text{el}}(\mathbf{C}\mathbf{C}_i^{-1}) + \psi_{\text{kin}}(\mathbf{C}_i\mathbf{C}_{ii}^{-1}) + \psi_{\text{iso}}(s - s_d).$$

### 2.6.2 Transformation of the potential relations for stresses

Recall that (cf. equation (9.60) in [12])

$$\mathbf{A}^T \frac{\partial \alpha(\mathbf{ABA}^T)}{\partial (\mathbf{ABA}^T)} \mathbf{A} = \frac{\partial \alpha(\mathbf{ABA}^T)}{\partial \mathbf{B}} \Big|_{\mathbf{A}=\text{const}}. \quad (45)$$

On the other hand,

$$\tilde{\mathbf{T}} \stackrel{(20)_{2,(30)_{1}}}{=} 2\rho_R \mathbf{F}_i^{-1} \frac{\partial \psi_{\text{el}}(\hat{\mathbf{C}}_e)}{\partial \hat{\mathbf{C}}_e} \mathbf{F}_i^{-T}, \quad \tilde{\mathbf{X}} \stackrel{(23)_{1,(30)_{2}}}{=} 2\rho_R \mathbf{F}_{ii}^{-1} \frac{\partial \psi_{\text{kin}}(\check{\mathbf{C}}_{ie})}{\partial \check{\mathbf{C}}_{ie}} \mathbf{F}_{ii}^{-T}.$$

But,

$$\hat{\mathbf{C}}_e = \mathbf{F}_i^{-T} \mathbf{C} \mathbf{F}_i^{-1}, \quad \check{\mathbf{C}}_{ie} = \mathbf{F}_{ii}^{-T} \mathbf{C}_i \mathbf{F}_{ii}^{-1}.$$

Substituting  $\mathbf{F}_i^{-T}, \mathbf{C}, \hat{\mathbf{C}}_e$  and  $\mathbf{F}_{ii}^{-T}, \mathbf{C}_i, \check{\mathbf{C}}_{ie}$  for  $\mathbf{A}, \mathbf{B}, \mathbf{ABA}^T$  in (45), we obtain

$$\tilde{\mathbf{T}} = 2\rho_R \frac{\partial \psi_{\text{el}}(\mathbf{C}\mathbf{C}_i^{-1})}{\partial \mathbf{C}} \Big|_{\mathbf{C}_i=\text{const}}, \quad \tilde{\mathbf{X}} = 2\rho_R \frac{\partial \psi_{\text{kin}}(\mathbf{C}_i\mathbf{C}_{ii}^{-1})}{\partial \mathbf{C}_i} \Big|_{\mathbf{C}_{ii}=\text{const}}. \quad (46)$$

Now let us show that  $\mathbf{C}^T \tilde{\mathbf{T}}$  and  $\mathbf{C}_i \tilde{\mathbf{X}}$  are isotropic functions of  $\mathbf{C}\mathbf{C}_i^{-1}$  and  $\mathbf{C}_i\mathbf{C}_{ii}^{-1}$ , respectively. Indeed, note that

$$\frac{\partial \alpha(\mathbf{AB}^{-1})}{\partial \mathbf{A}} \Big|_{\mathbf{B}=\text{const}} = \frac{\partial \alpha(\mathbf{AB}^{-1})}{\partial (\mathbf{AB}^{-1})} \mathbf{B}^{-1}, \quad \frac{\partial J_k(\mathbf{A})}{\partial \mathbf{A}} = (\mathbf{A}^T)^{k-1}, \quad k = 1, 2, 3. \quad (47)$$

Combining (46) and (47), we get

$$\mathbf{C}\tilde{\mathbf{T}} = 2\rho_{\text{R}} \sum_{k=1}^3 \frac{\partial\psi_{\text{el}}}{\partial J_k(\mathbf{C}\mathbf{C}_i^{-1})} (\mathbf{C}\mathbf{C}_i^{-1})^k, \quad \mathbf{C}_i\tilde{\mathbf{X}} = 2\rho_{\text{R}} \sum_{k=1}^3 \frac{\partial\psi_{\text{kin}}}{\partial J_k(\mathbf{C}_i\mathbf{C}_{\text{ii}}^{-1})} (\mathbf{C}_i\mathbf{C}_{\text{ii}}^{-1})^k.$$

If the special form (26), (27) for the free energy is used, then, taking into account incompressibility relations (43), we obtain

$$\tilde{\mathbf{T}} = k \ln\sqrt{\det(\mathbf{C})} \mathbf{C}^{-1} + \mu \mathbf{C}^{-1}(\overline{\mathbf{C}}\mathbf{C}_i^{-1})^{\text{D}}, \quad \tilde{\mathbf{X}} = \frac{c}{2} \mathbf{C}_i^{-1}(\mathbf{C}_i\mathbf{C}_{\text{ii}}^{-1})^{\text{D}}. \quad (48)$$

### 2.6.3 Representation of $\|\hat{\Sigma}^{\text{D}}\|$

First, let us note that

$$\text{tr}\hat{\Sigma} = \text{tr}(\hat{\mathbf{C}}_e\hat{\mathbf{S}} - \hat{\mathbf{X}}) = \text{tr}(\mathbf{C}\tilde{\mathbf{T}} - \mathbf{C}_i\tilde{\mathbf{X}}). \quad (49)$$

Next, we compute the inelastic contravariant and covariant pull-back of  $\hat{\Sigma}^{\text{D}}$

$$(\mathbf{F}_i^{-\text{T}})^* \hat{\Sigma}^{\text{D}} = \mathbf{C}_i^{-1}\mathbf{C}\tilde{\mathbf{T}} - \tilde{\mathbf{X}} - \text{tr}\hat{\Sigma} \mathbf{C}_i^{-1} \stackrel{(49)}{=} \mathbf{C}_i^{-1}(\mathbf{C}\tilde{\mathbf{T}} - \mathbf{C}_i\tilde{\mathbf{X}})^{\text{D}}, \quad (50)$$

$$(\mathbf{F}_i)^* \hat{\Sigma}^{\text{D}} = \mathbf{C}\tilde{\mathbf{T}}\mathbf{C}_i - \mathbf{C}_i\tilde{\mathbf{X}}\mathbf{C}_i - \text{tr}\hat{\Sigma} \mathbf{C}_i \stackrel{(49)}{=} (\mathbf{C}\tilde{\mathbf{T}} - \mathbf{C}_i\tilde{\mathbf{X}})^{\text{D}}\mathbf{C}_i. \quad (51)$$

Furthermore, since  $\hat{\Sigma}^{\text{D}} \in \text{Sym}$ , we get

$$\|\hat{\Sigma}^{\text{D}}\|^2 = \text{tr}(\hat{\Sigma}^{\text{D}}\hat{\Sigma}^{\text{D}}) = \text{tr}\left\{\left[(\mathbf{F}_i^{-\text{T}})^* \hat{\Sigma}^{\text{D}}\right]\left[(\mathbf{F}_i)^* \hat{\Sigma}^{\text{D}}\right]\right\}. \quad (52)$$

Substituting (50) and (51) in (52) we obtain the norm of the driving force

$$\mathfrak{F} := \|\hat{\Sigma}^{\text{D}}\| = \sqrt{\text{tr}\left[(\mathbf{C}\tilde{\mathbf{T}} - \mathbf{C}_i\tilde{\mathbf{X}})^{\text{D}}\right]^2}. \quad (53)$$

### 2.6.4 Transformation of the evolution equations

Note that

$$\text{tr}\check{\Xi} = \text{tr}(\check{\mathbf{C}}_{\text{ie}}\check{\mathbf{X}}) = \text{tr}(\mathbf{C}_i\tilde{\mathbf{X}}). \quad (54)$$

Next, we compute the covariant pull-back of  $\check{\Xi}^{\text{D}}$  :

$$(\mathbf{F}_{\text{ii}})^* \check{\Xi}^{\text{D}} \stackrel{(54)}{=} (\mathbf{C}_i\tilde{\mathbf{X}})^{\text{D}}\mathbf{C}_{\text{ii}}. \quad (55)$$

Covariant Pull-back of (39) yields

$$\dot{\mathbf{C}}_i = 2(\mathbf{F}_i)^* \hat{\Gamma}_i \stackrel{(39)}{=} 2\frac{\lambda_i}{\mathfrak{F}}(\mathbf{F}_i)^* \hat{\Sigma}^{\text{D}}, \quad \dot{\mathbf{C}}_{\text{ii}} = 2(\mathbf{F}_{\text{ii}})^* \hat{\Gamma}_{\text{ii}} \stackrel{(39)}{=} 2\lambda_{\text{ii}}\check{\Xi}^{\text{D}}.$$

Table 1

Summary of the material model

$\dot{\mathbf{C}}_i = 2\frac{\lambda_i}{\mathfrak{F}}(\mathbf{C}\tilde{\mathbf{T}} - \mathbf{C}_i\tilde{\mathbf{X}})^D \mathbf{C}_i,$	$\mathbf{C}_i _{t=0} = \mathbf{C}_i^0, \det \mathbf{C}_i^0 = 1,$
$\dot{\mathbf{C}}_{ii} = 2\lambda_i \varkappa(\mathbf{C}_i\tilde{\mathbf{X}})^D \mathbf{C}_{ii},$	$\mathbf{C}_{ii} _{t=0} = \mathbf{C}_{ii}^0, \det \mathbf{C}_{ii}^0 = 1,$
$\dot{s} := \sqrt{\frac{2}{3}}\lambda_i, \quad \dot{s}_d := \frac{\beta}{\gamma}\dot{\gamma}R,$	$s _{t=0} = s^0, \quad s_d _{t=0} = s_d^0,$
$\tilde{\mathbf{T}} = 2\rho_R \frac{\partial \psi_{el}(\mathbf{C}\mathbf{C}_i^{-1})}{\partial \mathbf{C}} \Big _{\mathbf{C}_i = \text{const}},$	$\tilde{\mathbf{X}} = 2\rho_R \frac{\partial \psi_{kin}(\mathbf{C}_i\mathbf{C}_{ii}^{-1})}{\partial \mathbf{C}_i} \Big _{\mathbf{C}_{ii} = \text{const}},$
$R = \gamma s_e, \quad s_e = s - s_d,$	
$\lambda_i := \frac{1}{\eta} \left\langle \frac{1}{k_0} f \right\rangle^m, \quad f = \mathfrak{F} - \sqrt{\frac{2}{3}}[K + R], \quad \mathfrak{F} = \sqrt{\text{tr}[(\mathbf{C}\tilde{\mathbf{T}} - \mathbf{C}_i\tilde{\mathbf{X}})^D]^2}.$	

Combining this with (51) and (55), we obtain

$$\dot{\mathbf{C}}_i = 2\frac{\lambda_i}{\mathfrak{F}}(\mathbf{C}\tilde{\mathbf{T}} - \mathbf{C}_i\tilde{\mathbf{X}})^D \mathbf{C}_i, \quad \dot{\mathbf{C}}_{ii} = 2\lambda_i \varkappa(\mathbf{C}_i\tilde{\mathbf{X}})^D \mathbf{C}_{ii}. \quad (56)$$

The material model is summarized in table 1.

### 3 Integration algorithms

The exact solution of (56) has under proper initial conditions the following geometric property:  $\mathbf{C}_i, \mathbf{C}_{ii}$  lie on the manifold  $\mathbb{M}$ , defined by

$$\mathbb{M} := \left\{ \mathbf{B} \in \text{Sym} : \det \mathbf{B} = 1 \right\}. \quad (57)$$

Hence, system (56) is a *system of differential equations on the manifold* (cf. the paper [9]). In this section we analyse two numerical schemes, such that the numerical solution lies exactly on  $\mathbb{M}$ .

#### 3.1 Modified Euler-Backward and exponential scheme

Consider the Cauchy problem for a system of nonlinear ordinary differential equations

$$\dot{\mathbf{A}}(t) = \mathbf{f}(\mathbf{A}(t), t)\mathbf{A}(t), \quad \mathbf{A}(0) = \mathbf{A}^0, \quad \det(\mathbf{A}^0) = 1.$$

Suppose that the tensor-valued function  $\mathbf{f}$  is sufficiently smooth,  $\text{tr}(\mathbf{f}(\mathbf{B}, t)) = 0$  and

$$\left( \mathbf{f}(\mathbf{B}, t) \right)^k \mathbf{B} \in \text{Sym} \quad \forall \mathbf{B} \in \text{Sym}, \quad k = 1, 2, 3, \dots \quad (58)$$

Under such conditions the exact solution lies on  $\mathbb{M}$ .

*Remark:* condition (58) is nontrivial, since  $\mathbf{f}(\mathbf{B}, t)$  is, in general, an anisotropic function of  $\mathbf{B}$ .

By  ${}^n\mathbf{A}$ ,  ${}^{n+1}\mathbf{A}$  denote numerical solutions respectively at  $t_n$  and  $t_{n+1}$ ,  $\Delta t := t_{n+1} - t_n$ . Suppose that  ${}^n\mathbf{A} \in \mathbb{M}$  is given. The classical Euler-Backward method (EBM) uses the equation with respect to the unknown  ${}^{n+1}\mathbf{A}$  :

$${}^{n+1}\mathbf{A} = \left[ \mathbf{1} - \Delta t \mathbf{f}({}^{n+1}\mathbf{A}, t_{n+1}) \right]^{-1} {}^n\mathbf{A}. \quad (59)$$

Recall that for small  $\mathbf{B}$  <sup>5</sup>

$$\left[ \mathbf{1} - \mathbf{B} \right]^{-1} = \mathbf{1} + \mathbf{B} + \mathbf{B}^2 + \mathbf{B}^3 + \dots . \quad (60)$$

The exponential method (EM) is based on the equation

$${}^{n+1}\mathbf{A} = \exp \left( \Delta t \mathbf{f}({}^{n+1}\mathbf{A}, t_{n+1}) \right) {}^n\mathbf{A}, \quad (61)$$

where the tensor exponential is given by

$$\exp \left( \mathbf{B} \right) := \mathbf{1} + \mathbf{B} + \frac{1}{2!}\mathbf{B}^2 + \frac{1}{3!}\mathbf{B}^3 + \dots . \quad (62)$$

Let us show that *both methods yield a symmetric solution*. The idea of the proof is as follows. Substituting (60) for  $\left[ \mathbf{1} - \Delta t \mathbf{f}({}^{n+1}\mathbf{A}, t_{n+1}) \right]^{-1}$  in (59), and (62) for  $\exp \left( \Delta t \mathbf{f}({}^{n+1}\mathbf{A}, t_{n+1}) \right)$  in (61), we get for both methods

$${}^{n+1}\mathbf{A} = \mathbf{K}({}^{n+1}\mathbf{A}), \quad (63)$$

$$\mathbf{K}(\mathbf{B}) := \left( \mathbf{1} + \Delta t \mathbf{f}(\mathbf{B}, t_{n+1}) + \sum_{k=2}^{\infty} c_k \left( \mathbf{f}(\mathbf{B}, t_{n+1}) \right)^k \right) {}^n\mathbf{A}, \quad (64)$$

with some coefficients  $c_k$ . Next, let us consider an auxiliary problem

$$\mathbf{A}_{\text{aux}} = \text{sym}(\mathbf{K}(\mathbf{A}_{\text{aux}})). \quad (65)$$

Here, the symmetrization operator  $\text{sym}(\cdot) = \frac{1}{2} \left( (\cdot) + (\cdot)^T \right)$  is used. Suppose  $\mathbf{A}_{\text{aux}}$  is a solution of (65). According to properties (58), since  $\mathbf{A}_{\text{aux}}$  is symmetric, we obtain

$$\mathbf{A}_{\text{aux}} {}^n\mathbf{A}^{-1} \mathbf{A}_{\text{aux}} \in \text{Sym}, \quad \mathbf{K}(\mathbf{A}_{\text{aux}}) {}^n\mathbf{A}^{-1} \mathbf{A}_{\text{aux}} \in \text{Sym}. \quad (66)$$

Subtracting (66)<sub>1</sub> from (66)<sub>2</sub> and taking (65) into account, we get

$$\text{skew} \left( \mathbf{K}(\mathbf{A}_{\text{aux}}) \right) {}^n\mathbf{A}^{-1} \mathbf{A}_{\text{aux}} \in \text{Sym}, \quad \text{skew}(\cdot) := (\cdot) - \text{sym}(\cdot). \quad (67)$$

Here  $\text{skew}(\cdot)$  stands for the skew-symmetric part of a tensor. Thus, (67)<sub>1</sub> yields

$$\text{skew} \left( \text{skew} \left( \mathbf{K}(\mathbf{A}_{\text{aux}}) \right) {}^n\mathbf{A}^{-1} \mathbf{A}_{\text{aux}} \right) = \mathbf{0}. \quad (68)$$

<sup>5</sup> The Neumann series (60) converges if  $\|\mathbf{B}\|^* < 1$ .



Since  $\text{skew skew}(\cdot) = \text{skew}(\cdot)$ , from (68) follows

$$\text{skew}\left(\mathbf{K}(\mathbf{A}_{\text{aux}})\right) = \text{skew}\left(\text{skew}\left(\mathbf{K}(\mathbf{A}_{\text{aux}})\right) \left(\mathbf{1} - {}^n\mathbf{A}^{-1} \mathbf{A}_{\text{aux}}\right)\right). \quad (69)$$

Denote by  $\|\cdot\|^*$  an induced norm of a tensor

$$\|\mathbf{B}\|^* := \max_{\|\mathbf{x}\|_2=1} \|\mathbf{B}\mathbf{x}\|_2, \quad \|\mathbf{x}\|_2 := \sqrt{x_1^2 + x_2^2 + x_3^2}. \quad (70)$$

Then,

$$\|\mathbf{A}\mathbf{B}\|^* \leq \|\mathbf{A}\|^* \|\mathbf{B}\|^*, \quad \|\text{skew}(\mathbf{A})\|^* \leq \|\mathbf{A}\|^*. \quad (71)$$

Note also that for small  $\Delta t$

$$\|\mathbf{1} - {}^n\mathbf{A}^{-1} \mathbf{A}_{\text{aux}}\|^* \leq \frac{1}{2}. \quad (72)$$

Taking the norm of both sides of (69) and using (71), (72), we get

$$\begin{aligned} \|\text{skew}\left(\mathbf{K}(\mathbf{A}_{\text{aux}})\right)\|^* &\stackrel{(69),(71)_2}{\leq} \left\| \text{skew}\left(\mathbf{K}(\mathbf{A}_{\text{aux}})\right) \left(\mathbf{1} - {}^n\mathbf{A}^{-1} \mathbf{A}_{\text{aux}}\right) \right\|^* \\ &\stackrel{(71)_1}{\leq} \|\text{skew}\left(\mathbf{K}(\mathbf{A}_{\text{aux}})\right)\|^* \|\mathbf{1} - {}^n\mathbf{A}^{-1} \mathbf{A}_{\text{aux}}\|^* \stackrel{(72)}{\leq} \frac{1}{2} \|\text{skew}\left(\mathbf{K}(\mathbf{A}_{\text{aux}})\right)\|^*. \end{aligned}$$

This implies that  $\|\text{skew}\left(\mathbf{K}(\mathbf{A}_{\text{aux}})\right)\|^* = 0$ . Therefore,  $\mathbf{K}(\mathbf{A}_{\text{aux}}) \in \text{Sym}$  and  $\mathbf{A}_{\text{aux}}$  is a solution of (63). In other words, equations (63) and (65) are *equivalent*. ■

This means that *no modifications of (59) and (61) are necessary* to ensure the symmetry of the solution  ${}^{n+1}\mathbf{A}$ . The reader will have no difficulty in showing that *the problem of symmetry does not occur* also for a system of equations of type (63), (64).

The following modifications of equations (59) and (61) leave the corresponding original solutions unchanged:

$${}^{n+1}\mathbf{A} = \text{sym}\left\{ \left[ \mathbf{1} - \Delta t \mathbf{f}({}^{n+1}\mathbf{A}, t_{n+1}) \right]^{-1} {}^n\mathbf{A} \right\}, \quad (73)$$

$${}^{n+1}\mathbf{A} = \text{sym}\left\{ \exp\left(\Delta t \mathbf{f}({}^{n+1}\mathbf{A}, t_{n+1})\right) {}^n\mathbf{A} \right\}. \quad (74)$$

The advantage of the exponential method based on (61) or (74) is that the constraint  $\det({}^{n+1}\mathbf{A}) = 1$  is exactly satisfied. In this paper we modify the right-hand side of (59) and (73), using the projection  $\overline{(\cdot)} = (\det(\cdot))^{-1/3}(\cdot)$  on the group of unimodular tensors (cf. [14]):

$${}^{n+1}\mathbf{A} = \overline{\left[ \mathbf{1} - \Delta t \mathbf{f}({}^{n+1}\mathbf{A}, t_{n+1}) \right]^{-1} {}^n\mathbf{A}}, \quad (75)$$

$${}^{n+1}\mathbf{A} = \overline{\text{sym}\left\{ \left[ \mathbf{1} - \Delta t \mathbf{f}({}^{n+1}\mathbf{A}, t_{n+1}) \right]^{-1} {}^n\mathbf{A} \right\}}. \quad (76)$$

Let us remark that both (75) and (76) yield the same solution  ${}^{n+1}\mathbf{A} \in \mathbb{M}$ . Thus, the modified Euler-Backward (MEBM) is formulated by (75) or (76). Further, we notice that

the exponential method (EM) (61) is equivalent to

$${}^{n+1}\mathbf{A} = \overline{\text{sym}\left\{\exp\left(\Delta t \mathbf{f}({}^{n+1}\mathbf{A}, t_{n+1})\right) {}^n\mathbf{A}\right\}}. \quad (77)$$

*Remark.* We have a freedom in choosing between (75) and (76) for MEBM. Similarly, the EM can be based either on (61) or (77). In this paper we use symmetrized equations (76), (77). The reason is that these two equations can be formulated with respect to six real unknowns. At the same time equations (75), (61) are formulated with respect to nine independent real unknowns.

### 3.2 Adaptation of integration methods to the evolution equations

Suppose that the deformation gradient  ${}^{n+1}\mathbf{F}$  at the time  $t_{n+1} = t_n + \Delta t$  is known. Further, assume that the internal variables  $\mathbf{C}_i, \mathbf{C}_{ii}, s, s_d$  at the time  $t_n$  are given by  ${}^n\mathbf{C}_i, {}^n\mathbf{C}_{ii}, {}^n s, {}^n s_d$ , respectively. In this subsection we formulate a system of equations for finding the internal variables at the time  $t_{n+1}$ .

First, we adopt the modified Euler-Backward scheme (76) and the exponential scheme (77) to the numerical integration of evolution equations (56). We stress that the right-hand sides in (56) satisfy requirements (58). For instance, let us analyse the evolution equation for  $\mathbf{C}_i$ . Note that, since  $\mathbf{C}\tilde{\mathbf{T}}$  and  $\mathbf{C}_i\tilde{\mathbf{X}}$  are isotropic functions of  $\mathbf{C}\mathbf{C}_i^{-1}$  and  $\mathbf{C}_i\mathbf{C}_{ii}^{-1}$ ,

$$2\frac{\lambda_i}{\mathfrak{F}}\left(\mathbf{C}\tilde{\mathbf{T}} - \mathbf{C}_i\tilde{\mathbf{X}}\right)^D = d_1\mathbf{1} + d_2\mathbf{C}\mathbf{C}_i^{-1} + d_3(\mathbf{C}\mathbf{C}_i^{-1})^2 + d_4\mathbf{C}_i\mathbf{C}_{ii}^{-1} + d_5(\mathbf{C}_i\mathbf{C}_{ii}^{-1})^2,$$

with some suitable  $d_n \in \mathbb{R}$ . It remains to check that

$$(\mathbf{C}\mathbf{C}_i^{-1})^k \mathbf{C}_i \in \text{Sym}, \quad (\mathbf{C}_i\mathbf{C}_{ii}^{-1})^k \mathbf{C}_i \in \text{Sym}, \quad \forall \mathbf{C}_i, \mathbf{C}_{ii} \in \text{Sym}, \quad k = 1, 2, 3, \dots$$

The evolution equations for  $s, s_d$  are discretized by implicit Euler scheme. Further, consider an incremental inelastic parameter

$$\xi := \Delta t {}^{n+1}\lambda_i. \quad (78)$$

Finally, we get the following system of equations.

$${}^{n+1}\mathbf{C}_i - \overline{\text{sym}\left(\mathbf{K}_i({}^{n+1}\mathbf{C}, {}^{n+1}\mathbf{C}_i, {}^{n+1}\mathbf{C}_{ii}, \xi)\right)} = \mathbf{0}, \quad (79)$$

$${}^{n+1}\mathbf{C}_{ii} - \overline{\text{sym}\left(\mathbf{K}_{ii}({}^{n+1}\mathbf{C}_i, {}^{n+1}\mathbf{C}_{ii}, \xi)\right)} = \mathbf{0}, \quad (80)$$

$$\xi = \frac{\Delta t}{\eta} \left\langle \frac{{}^{n+1}f}{k_0} \right\rangle^m, \quad (81)$$

$${}^{n+1}s = {}^n s + \sqrt{\frac{2}{3}}\xi, \quad {}^{n+1}s_d = {}^n s_d + \frac{\beta}{\gamma}\sqrt{\frac{2}{3}}\xi {}^{n+1}R, \quad (82)$$

$${}^{n+1}R = \gamma({}^{n+1}s - {}^{n+1}s_d), \quad {}^{n+1}f = {}^{n+1}\mathfrak{F} - \sqrt{\frac{2}{3}}(K + {}^{n+1}R), \quad (83)$$

$${}^{n+1}\mathfrak{F} = \sqrt{\text{tr}\left[\left({}^{n+1}\mathbf{C} \quad {}^{n+1}\tilde{\mathbf{T}} - {}^{n+1}\mathbf{C}_i \quad {}^{n+1}\tilde{\mathbf{X}}\right)^{\text{D}}\right]^2}, \quad (84)$$

where the operators  $\mathbf{K}_k$ ,  $k \in \{i, ii\}$  are defined by

$$\mathbf{K}_k := \begin{cases} [\mathbf{1} - \mathbf{B}_k]^{-1} {}^n \mathbf{C}_k & \text{if MEBM is employed} \\ \exp[\mathbf{B}_k] {}^n \mathbf{C}_k & \text{if EM is employed} \end{cases},$$

$$\mathbf{B}_i({}^{n+1}\mathbf{C}, {}^{n+1}\mathbf{C}_i, {}^{n+1}\mathbf{C}_{ii}, \xi) := 2\frac{\xi}{{}^{n+1}\mathfrak{F}}\left({}^{n+1}\mathbf{C} \quad {}^{n+1}\tilde{\mathbf{T}} - {}^{n+1}\mathbf{C}_i \quad {}^{n+1}\tilde{\mathbf{X}}\right)^{\text{D}}, \quad (85)$$

$$\mathbf{B}_{ii}({}^{n+1}\mathbf{C}_i, {}^{n+1}\mathbf{C}_{ii}, \xi) := 2\xi \mathcal{X}\left({}^{n+1}\mathbf{C}_i \quad {}^{n+1}\tilde{\mathbf{X}}\right)^{\text{D}}. \quad (86)$$

Here  ${}^{n+1}\tilde{\mathbf{T}}$ ,  ${}^{n+1}\tilde{\mathbf{X}}$  are functions of  ${}^{n+1}\mathbf{C}$ ,  ${}^{n+1}\mathbf{C}_i$ ,  ${}^{n+1}\mathbf{C}_{ii}$ , given by (46) (or by (48) if the special form of  $\psi_{\text{el}}$ ,  $\psi_{\text{kin}}$  is used).

### 3.3 Solution strategy

First, we exclude  ${}^{n+1}s$ ,  ${}^{n+1}s_d$  from (82), (83)<sub>1</sub> (cf. [14]) to get

$${}^{n+1}R = R(\xi) := \frac{{}^t R + \sqrt{\frac{2}{3}}\gamma\xi}{1 + \sqrt{\frac{2}{3}}\beta\xi}, \quad {}^t R := \gamma({}^n s - {}^n s_d). \quad (87)$$

Next, substituting (84) and (87) in (83)<sub>2</sub>, we represent  ${}^{n+1}f$  as a function of  ${}^{n+1}\mathbf{C}_i$ ,  ${}^{n+1}\mathbf{C}_{ii}$ ,  $\xi$ . Thus, the problem is reduced to system (79), (80), (81) with respect to  ${}^{n+1}\mathbf{C}_i$ ,  ${}^{n+1}\mathbf{C}_{ii}$ ,  $\xi$ .

In this paper we decompose problem (79), (80), (81) as follows. The variables  ${}^{n+1}\mathbf{C}_i$ ,  ${}^{n+1}\mathbf{C}_{ii}$  are uniquely determined by system (79), (80) with a given  $\xi$ . Let us denote the corresponding solution by  $(\mathbf{C}_i({}^{n+1}\mathbf{C}, \xi), \mathbf{C}_{ii}({}^{n+1}\mathbf{C}, \xi))$ . Substituting this solution in (84), we obtain a function  $\mathfrak{F}({}^{n+1}\mathbf{C}, \xi)$ .

If  $\mathfrak{F}({}^{n+1}\mathbf{C}, 0) - \sqrt{\frac{2}{3}}(K + {}^t R) \leq 0$ , then we put  $\xi := 0$ ,  ${}^{n+1}\mathbf{C}_i := {}^n \mathbf{C}_i$ ,  ${}^{n+1}\mathbf{C}_{ii} := {}^n \mathbf{C}_{ii}$  (no inelastic flow occurs). Otherwise,  $\xi$  is computed using equation (81). Substituting (83)<sub>2</sub> for  ${}^{n+1}f$  in (81), we obtain two alternative forms of the incremental consistency condition:

$$H({}^{n+1}\mathbf{C}, \xi) := \frac{\eta\xi}{\Delta t} - \left(\frac{\mathfrak{F}({}^{n+1}\mathbf{C}, \xi) - \sqrt{\frac{2}{3}}(K + R(\xi))}{k_0}\right)^m = 0, \quad (88)$$

$$D({}^{n+1}\mathbf{C}, \xi) := \left(\frac{\eta\xi}{\Delta t}\right)^{1/m} - \frac{\mathfrak{F}({}^{n+1}\mathbf{C}, \xi) - \sqrt{\frac{2}{3}}(K + R(\xi))}{k_0} = 0. \quad (89)$$

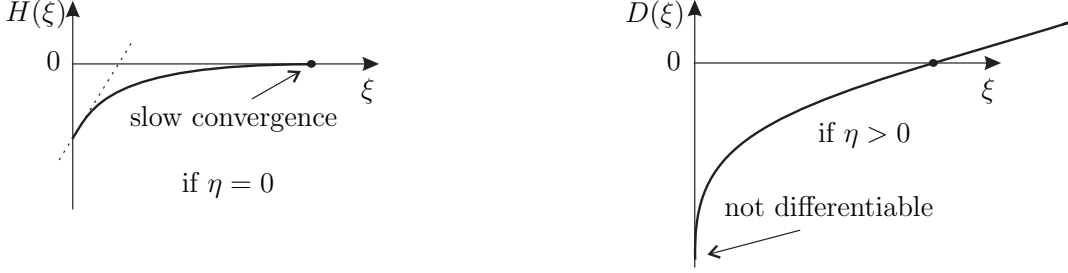


Fig. 2. Finding  $\xi$ .

After the solution  $\xi$  is found, the values of  ${}^{n+1}\mathbf{C}_i$ ,  ${}^{n+1}\mathbf{C}_{ii}$  are given by  $\mathbf{C}_i({}^{n+1}\mathbf{C}, \xi)$ ,  $\mathbf{C}_{ii}({}^{n+1}\mathbf{C}, \xi)$ . Finally, we update  $s$  and  $s_d$  using equations (82).

*Remark:* Solving system (81), (83)<sub>2</sub> with respect to  $\xi$  with a given  $\mathfrak{F}$ , it is possible to represent  $\xi$  as a function of  ${}^{n+1}\mathbf{C}_i$ ,  ${}^{n+1}\mathbf{C}_{ii}$ , thus reducing the number of unknowns. On the other hand, for small  $\eta$  this approach will result in an ill-posed problem.

### 3.4 Numerical implementation

The Newton-Raphson method is used to compute  $(\mathbf{C}_i({}^{n+1}\mathbf{C}, \xi), \mathbf{C}_{ii}({}^{n+1}\mathbf{C}, \xi))$  from (79), (80). To this end, equations (79), (80) are linearized analytically using the coordinate-free tensor formalism proposed by Itskov (see [16], [17]).

Notice that the straightforward application of Newton's method to the solution of (88) or (89) is not trivial. Indeed, for  $\eta = 0$ ,  $m > 1$ , the convergence of the Newton method for (88) fails to be quadratic since the first derivative is zero at the root (see fig. 2). At the same time, for  $\eta > 0$ , the initial approximation  $\xi^{(0)} = 0$  can not be used to compute the solution of (89), since the function  $D(\xi)$  is not differentiable at zero (see fig. 2). To overcome these difficulties, the first Newton iteration is performed using (88) with initial approximation  $\xi^{(0)} = 0$ , and the subsequent iterations are performed using (89).

The derivative  $\frac{\partial \mathfrak{F}({}^{n+1}\mathbf{C}, \xi)}{\partial \xi}$ , required by the Newton method, is calculated using the implicit differentiation of (79), (80) with respect to  $\xi$ . An alternative strategy is to solve (89) with the help of a derivative-free iteration scheme like Pegasus method [7], [20]. This approach is reasonable being combined with a fixed-point iteration for finding  $(\mathbf{C}_i({}^{n+1}\mathbf{C}, \xi), \mathbf{C}_{ii}({}^{n+1}\mathbf{C}, \xi))$ , such that no linearization of (79), (80) is required.

We implement the coordinate-free tensor formalism to obtain an analytical expression for the consistent tangent operator  $\frac{\partial {}^{n+1}\tilde{\mathbf{T}}}{\partial {}^{n+1}\mathbf{C}}$ . Using a special product  $\mathbf{A} \times \mathbf{B}$  of two second-rank tensors and the composition  $\mathbb{A} \mathbb{B}$  of two fourth-rank tensors (see definitions (2.6), (2.10)

in [17]), it follows from (46) that

$$\begin{aligned}\frac{\partial^{n+1}\tilde{\mathbf{T}}}{\partial^{n+1}\mathbf{C}} &= \frac{\partial\tilde{\mathbf{T}}^{(n+1)\mathbf{C}, n+1\mathbf{C}_i}}{\partial^{n+1}\mathbf{C}} + \frac{\partial\tilde{\mathbf{T}}^{(n+1)\mathbf{C}, n+1\mathbf{C}_i}}{\partial^{n+1}\mathbf{C}_i} \frac{\partial^{n+1}\mathbf{C}_i^{(n+1)\mathbf{C}}}{\partial^{n+1}\mathbf{C}}, \\ \frac{\partial^{n+1}\mathbf{C}_i^{(n+1)\mathbf{C}}}{\partial^{n+1}\mathbf{C}} &= \frac{\partial\mathbf{C}_i^{(n+1)\mathbf{C}, \xi}}{\partial^{n+1}\mathbf{C}} + \frac{\partial\mathbf{C}_i^{(n+1)\mathbf{C}, \xi}}{\partial\xi} \times \frac{\partial\xi^{(n+1)\mathbf{C}}}{\partial^{n+1}\mathbf{C}}, \\ \frac{\partial\xi^{(n+1)\mathbf{C}}}{\partial^{n+1}\mathbf{C}} &= -\left(\frac{\partial D^{(n+1)\mathbf{C}, \xi}}{\partial\xi}\right)^{-1} \frac{\partial D^{(n+1)\mathbf{C}, \xi}}{\partial^{n+1}\mathbf{C}}.\end{aligned}$$

The numerical computation of tensor exponential  $\exp(\mathbf{B})$  is performed using Taylor power series expansion (62). The derivative of tensor exponential is computed by (see [18])

$$\frac{\partial \exp(\mathbf{B})}{\partial \mathbf{B}} = \sum_{n=1}^{\infty} \frac{1}{n!} \sum_{k=0}^{n-1} \mathbf{B}^{n-1-k} \otimes \mathbf{B}^k.$$

In general, this approach fails due to the roundoff errors, and more sophisticated techniques are required (see, for example, [30], [18], [19], [25]). We do not use these advanced techniques in this paper, since in the present calculations the argument of the exponential function is bounded. Indeed, if  $\xi \leq 0.2$  then it follows from (85), (86) that

$$\|\mathbf{B}_k\| \approx 2\xi \leq 0.4, \quad k \in \{i, ii\}. \quad (90)$$

Therefore, the roundoff errors are negligible. Moreover, under condition (90), the truncated power series only with few terms yield exact results up to machine precision.

#### 4 Numerical tests

Now we analyse the accuracy of the integration methods presented in section 3. Toward this end, we simulate the material behaviour under strain controlled loading. The loading program in the time interval  $t \in [0, 300]$  is defined by

$$\mathbf{F}(t) = \overline{\mathbf{F}'(t)} \quad \text{or} \quad \mathbf{F}(t) = \mathbf{F}'(t), \quad (91)$$

where

$$\mathbf{F}'(t) := \begin{cases} (1 - t/100)\mathbf{F}_1 + (t/100)\mathbf{F}_2 & \text{if } t \in [0, 100] \\ (2 - t/100)\mathbf{F}_2 + (t/100 - 1)\mathbf{F}_3 & \text{if } t \in (100, 200] \\ (3 - t/100)\mathbf{F}_3 + (t/100 - 2)\mathbf{F}_4 & \text{if } t \in (200, 300] \end{cases},$$

with

$$\mathbf{F}_1 := \mathbf{1}, \quad \mathbf{F}_2 := \begin{pmatrix} 2 & 0 \\ 0 & \frac{1}{\sqrt{2}} & 0 \\ 0 & 0 & \frac{1}{\sqrt{2}} \end{pmatrix}, \quad \mathbf{F}_3 := \begin{pmatrix} 1 & 1 & 0 \\ 0 & 1 & 0 \\ 0 & 0 & 1 \end{pmatrix}, \quad \mathbf{F}_4 := \begin{pmatrix} \frac{1}{\sqrt{2}} & 0 \\ 0 & 2 & 0 \\ 0 & 0 & \frac{1}{\sqrt{2}} \end{pmatrix}.$$

*Remark.* In this section we test the numerical schemes under a variety of loading conditions, in particular, under non-proportional loading. In this connection, the loading program does not have to be mechanically plausible.

The material parameters used in simulations are summarized in table 2.

Table 2  
Material parameters

$k$ [MPa]	$\mu$ [MPa]	$c$ [MPa]	$\gamma$ [MPa]		
73500	28200	3500	460		
$K$ [MPa]	$m$ [-]	$\eta$ [s <sup>-1</sup> ]	$k_0$ [Mpa]	$\varkappa$ [MPa <sup>-1</sup> ]	$\beta$ [-]
270	3.6	$2 \cdot 10^6$	1	0.028	5

We put the following initial conditions on the internal variables

$$\mathbf{C}_i|_{t=0} = \mathbf{1}, \quad \mathbf{C}_{ii}|_{t=0} = \mathbf{1}, \quad s|_{t=0} = 0, \quad s_d|_{t=0} = 0. \quad (92)$$

Only the uniform time stepping is used in this paper. The numerical solution obtained with extremely small time step ( $\Delta t = 0.01$ s) will be named the *exact solution*.

The coordinates of Cauchy stress tensor  $\mathbf{T}$  for loadings  $(91)_1$  and  $(91)_2$  are plotted respectively in figures 3 and 4. Note that  $\det(\mathbf{F}) \equiv 1$  if  $(91)_1$  is used, and no hydrostatic stress occurs. On the other hand, relation  $(91)_2$  results in a large hydrostatic stress and a *finite elastic bulk strain*.

The numerical simulation shows that both MEBM and EM have a similar error. Both methods produce slightly different results for  $\Delta t = 10$  s when the inelastic increment  $\xi$  ranges up to about 17%.

## 5 Characterization of the material model

We investigate qualitatively the material response, predicted by the material model. The numerical computations simulate basic material testing experiments. Material parameters from table 2 and initial conditions (92) are used in this section.

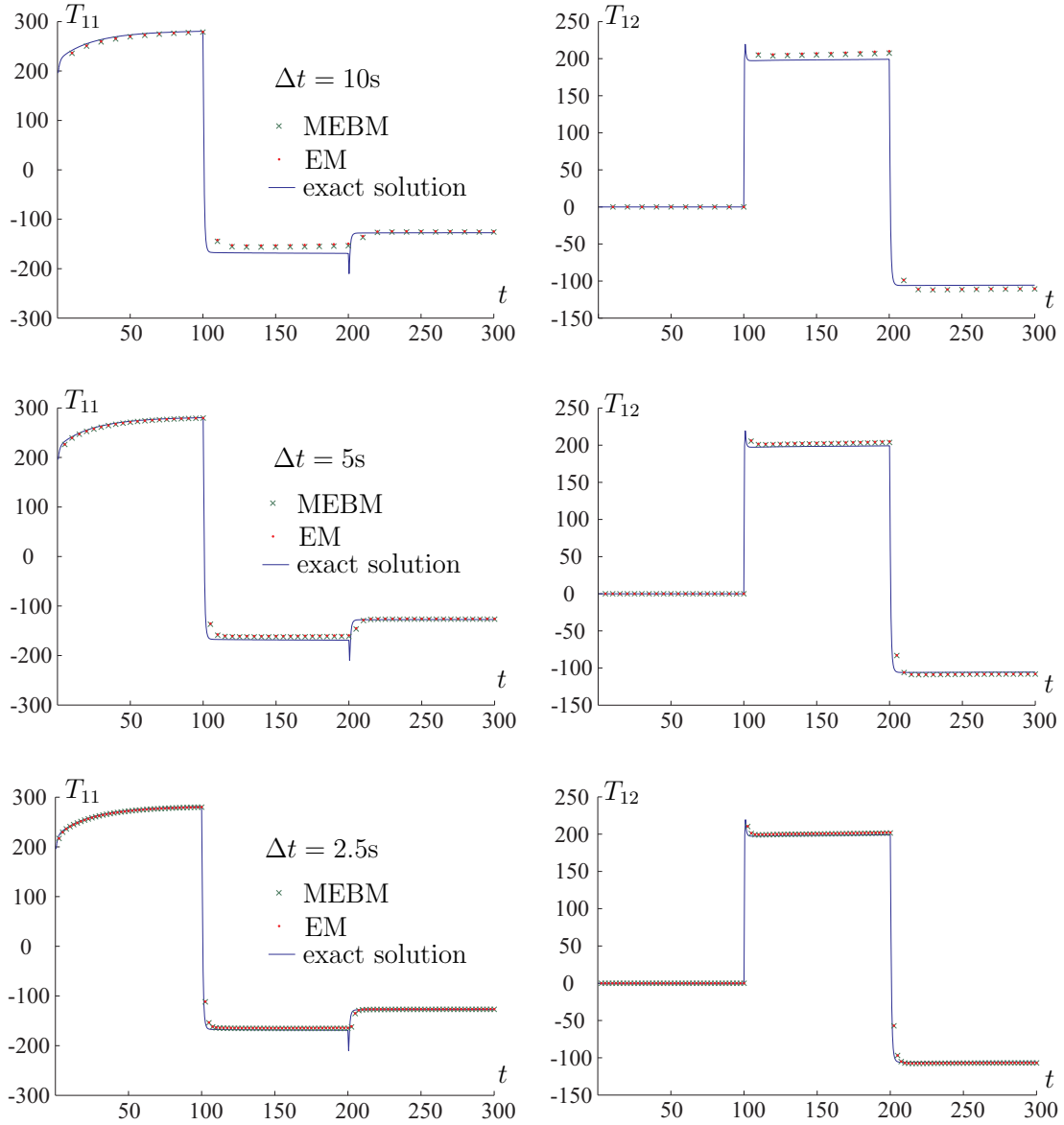


Fig. 3. Accuracy test with small elastic strains (use  $(91)_1$ ).

### 5.1 Uniaxial testing

For uniaxial test we put

$$\mathbf{F} = \begin{pmatrix} 1 + \varepsilon & 0 & 0 \\ 0 & \alpha & 0 \\ 0 & 0 & \alpha \end{pmatrix}, \quad T_{22} = T_{33} = 0. \quad (93)$$

The unknown  $\alpha$  is determined using  $(93)_2$ . The technical stress  $\sigma := \frac{A}{A_0}T_{11}$  is plotted in figure 5.a for various strain rates  $\dot{\varepsilon}$ . Here  $A$ ,  $A_0$  denote the current and initial cross

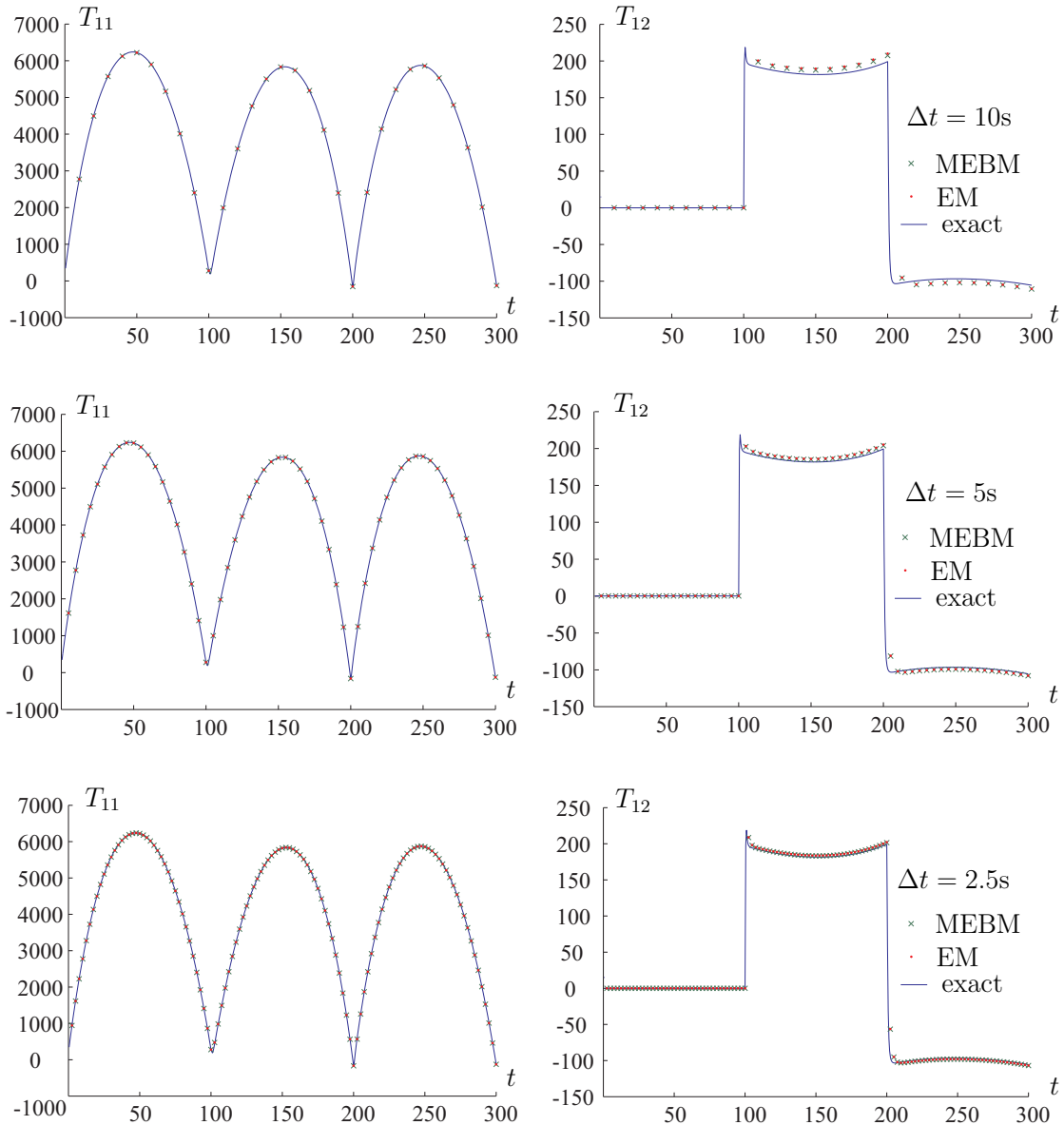


Fig. 4. Accuracy test with finite elastic strains (use  $(91)_2$ ).

sections, respectively. Although the material response is stable, the stress reduction is observed after the peak load in uniaxial monotonic test. The reason is the reduction of the cross-section. The equilibrium curve can be reached both by relaxation and creep (figure 5.b). In the simulation presented in figure 5.b each relaxation period lasts for 10 seconds. The creep time is 20 seconds. Therefore, the numerical experiment shows that it takes longer to reach equilibrium curve in the creep process than in the relaxation process. Finally, as indicated by the strain-controlled cyclic test (figure 5.c), the saturation is achieved after the isotropic hardening is accomplished.



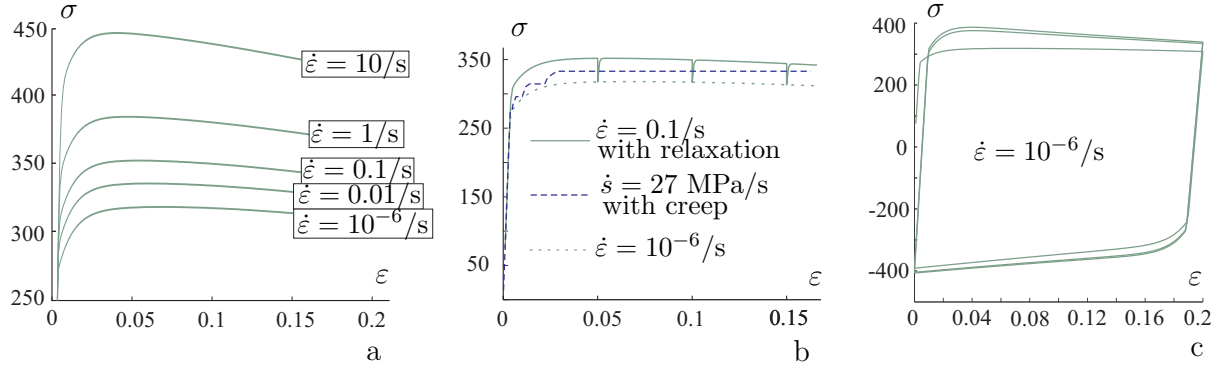


Fig. 5. Uniaxial testing: monotonic loading (a), relaxation and creep (b), and cyclic loading (c).

## 5.2 Torsion testing

The cyclic torsion testing has much potential for providing information about the non-linear hardening phenomena (see [8]). To simulate the torsion of constrained thin-walled tube we put

$$\mathbf{F} = \begin{pmatrix} 1 & \phi & 0 \\ 0 & 1 & 0 \\ 0 & 0 & \alpha \end{pmatrix}, \quad T_{33} = 0. \quad (94)$$

We consider a strain controlled torsion test with a given  $\phi$ ,  $|\dot{\phi}| = 0.01/s$ . The unknown  $\alpha$  is determined using  $(94)_2$ . Denote by  $\sigma := \frac{A}{A_0}T_{22}$  and  $\tau := \frac{A}{A_0}T_{12}$  the axial and shear stresses, respectively.

The axial stress  $\sigma$  is exactly zero in geometric linear theory. But, in the case of finite strains, so-called second order effects can appear, leading to nonzero axial stress. For instance, the Poynting effect (see [1]) is observed during the torsion of cylindrical samples made of aluminium alloy. This effect consists in axial compression of constrained samples or axial elongation of unconstrained samples (see [34]). The axial and shear stresses are plotted in figure 6 for different forming increments. As may be seen from the figure, the Poynting effect is predicted by the material model.

Next, as indicated by figure 6, the maximal stresses are influenced by the forming increment. For smaller forming increment the isotropic hardening is accomplished on the early stage of the forming process, thus leading to higher maximal stresses. On the other hand, if the kinematic hardening is not accomplished within one forming increment, a somewhat different material response is possible. For instance, the maximal stresses under the cyclic loading can be smaller than the stresses under the monotonic loading. In order to demonstrate this effect, we perform the numerical simulation (see figure 7) with modified hardening parameters:  $\varkappa := 0.0035 \text{ MPa}^{-1}$ ,  $c := 1500 \text{ MPa}$ ,  $\beta := 10$ ,  $\gamma := 1800 \text{ MPa}$ . A similar effect was reported in [27] for 20MoCr24 steel alloy.

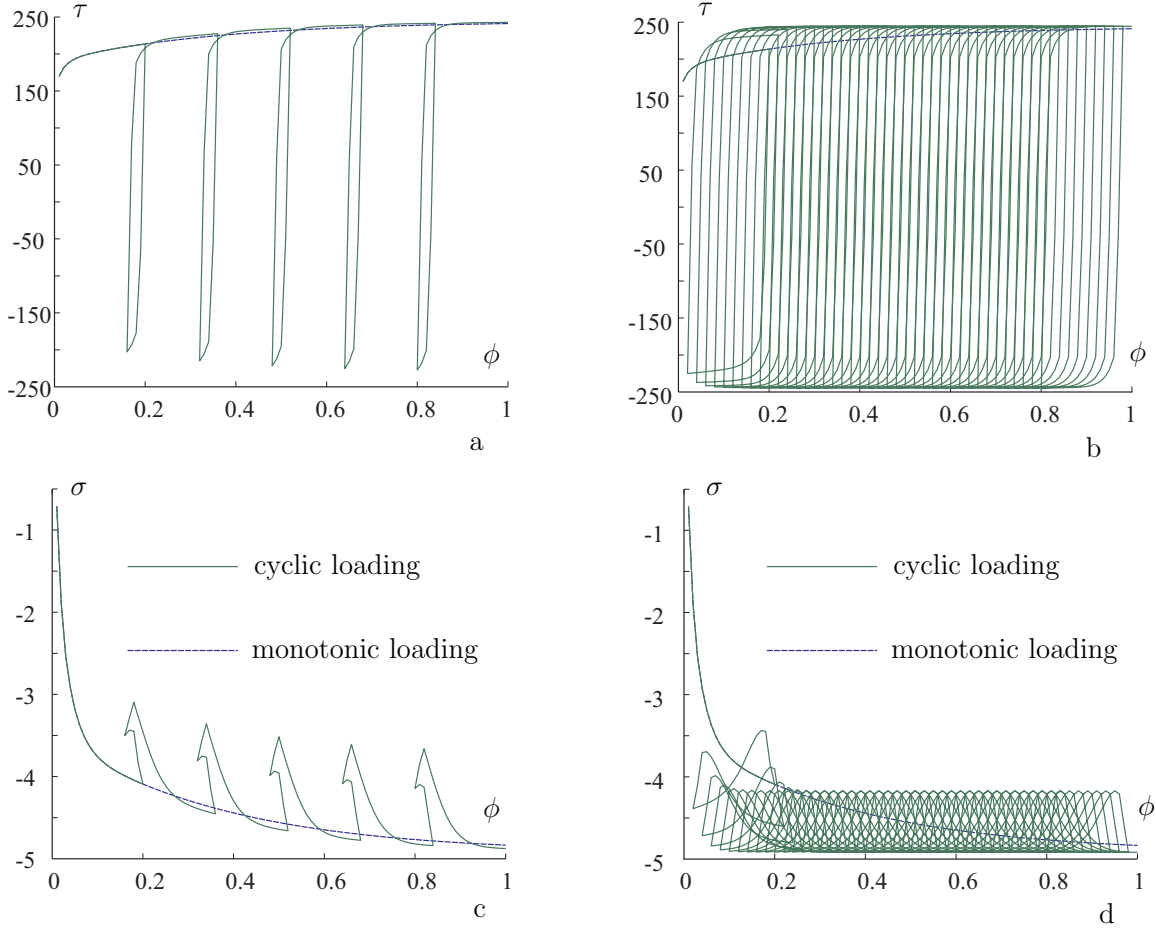


Fig. 6. Torsion testing (material parameters from table 2): shear stress (a), (b), and axial stress (c), (d).

## 6 Discussion

The classical material model of viscoplasticity is modified in a thermodynamically consistent manner to incorporate finite elastic and inelastic strains. The model takes rate-dependence (relaxation, creep) and hysteresis effects (nonlinear kinematic and isotropic hardening) into account.

Although the material response is anisotropic, the symmetry of  ${}^{n+1}\mathbf{C}_i$  and  ${}^{n+1}\mathbf{C}_{ii}$  is a priori preserved by EBM, MEBM and EM. It is shown that *no symmetrization procedure is necessary*. Moreover, any symmetrization should leave the corresponding solutions unchanged. Both MEBM and EM have the advantage that the inelastic incompressibility constraint is exactly satisfied.

Under special assumptions on the potential functions  $\psi_{el}$  and  $\psi_{kin}$  it may be beneficial to optimize the solution procedure of system (79) — (86), thus reducing the computational effort. On the other hand, the most important properties of any stress algorithm are stability, accuracy, robustness and universality. The computational effort, required for the

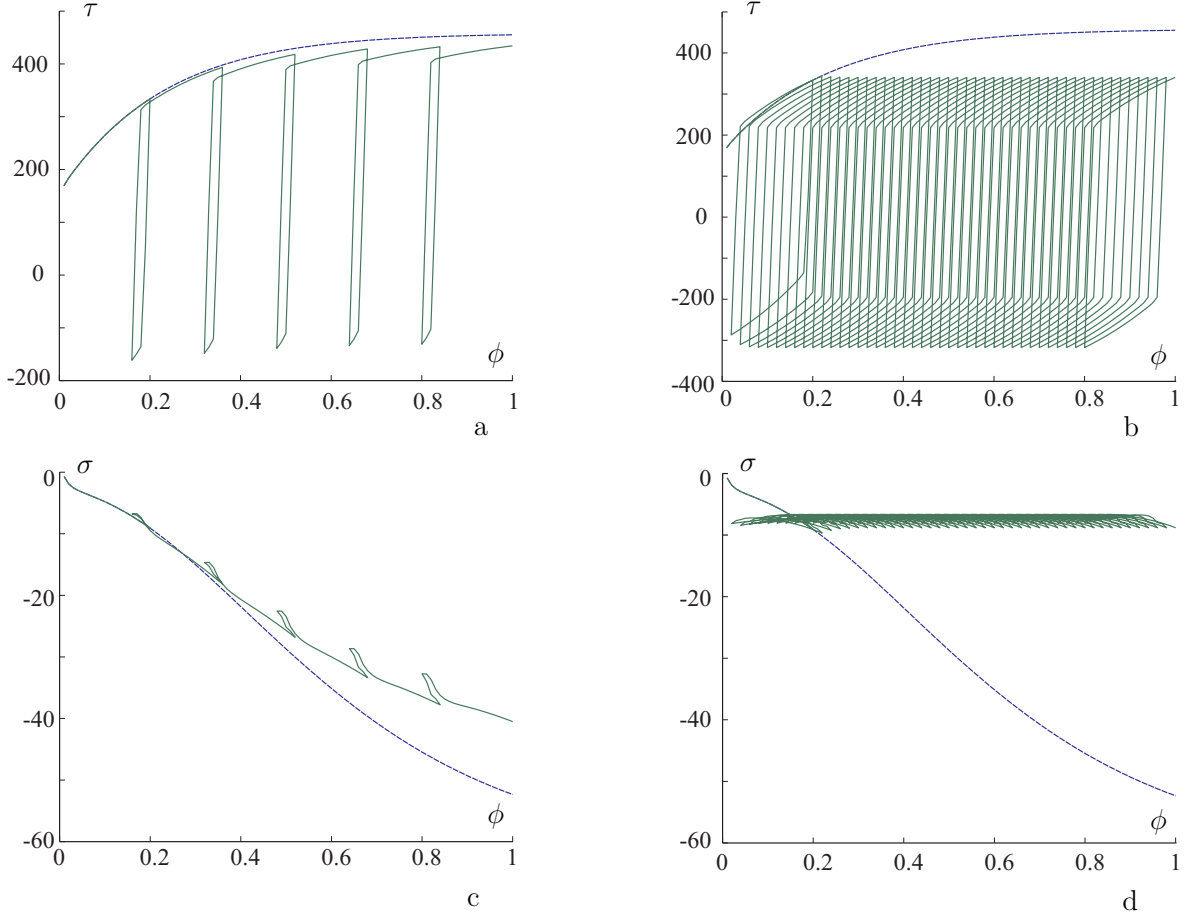


Fig. 7. Torsion testing (modified material parameters): shear stress (a), (b), and axial stress (c), (d).

evaluation of stresses and tangential operator, is negligible in comparison with the costs of solving the global linearized system of equations within the Newton-Raphson iterative procedure.

The material model reproduces qualitatively the experimental results [15], [28] for aluminium alloy processed by ECA-pressing. For more detailed modeling of kinematic hardening it is possible to introduce several Armstrong-Frederick terms, using series of multiplicative decompositions of type (3). To complete the phenomenological description of the material, a proper parameter identification is required.

## Acknowledgements

This research was supported by German National Science Foundation (DFG) within the collaborative research center SFB 692 "High-strength aluminium based light weight materials for reliable components". The authors are grateful to Dr. D. Helm and Dr. P. Neff for fruitful discussions.

## References

- [1] I. N. Andronov, N. P. Bogdanov, V. P. Vlasov, V. A. Likhachev, Laws governing the axial deformation of metals subjected to plastic torsion, *Strength of Materials*, 22, 7 (1990) 1046–1048.
- [2] P. J. Armstrong, C. O. Frederick, A mathematical representation of the multiaxial Bauschinger effect, Technical Report RD/B/N731, G.E.G.B, 1966.
- [3] J. L. Chaboche, G. Rousselier, On the Plastic and Viscoplastic Constitutive Equations, Part I: Rules Developed with Internal Variable Concept. *Journal of Pressure Vessel Technology*, ASME, 105 (1983) 153–158.
- [4] J. Chaboche, Constitutive equations for cyclic plasticity and cyclic viscoplasticity, *International Journal of Plasticity*, 5 (1989) 247–302.
- [5] W. Dettmer, S. Reese, On the theoretical and numerical modelling of Armstrong-Frederick kinematic hardening in the finite strain regime, *Computer Methods in Applied Mechanics and Engineering*, 193 (2004) 87-116.
- [6] A. Dogui, F. Sidoroff, Kinematic hardening in large elastoplastic strain, *Engineering Fracture Mechanics*, 21, 4 (1985) 685–695.
- [7] M. Dowell, P. Jarrat, The "Pegasus" method for computing the root of an equation, *BIT Numerical Mathematics*, 12 (1972) 503–508.
- [8] U. J. Görke, A. Bucher, R. Kreißig, A study on kinematic hardening models for the simulation of cyclic loading in finite elasto-plasticity based on a substructure approach, In: Owen, D.R.J., Onate, E. and Suarez, B. (Eds.): *Computational Plasticity: Fundamentals and Applications*. Proceedings of COMPLAS VIII, CIMNE Barcelona, (2005) 723–726.
- [9] E. Hairer, Geometric Integration of Ordinary Differential Equations on Manifolds, *BIT Numerical Mathematics*, 41, 5 (2001) 996–1007.
- [10] S. Hartmann, G. Lührs, P. Haupt, An efficient stress algorithm with applications in viscoplasticity and plasticity, *International Journal for Numerical Methods in Engineering*, 40 (1997) 991–1013.
- [11] P. Haupt, Ch. Tsakmakis, On the application of dual variables in continuum mechanics, *Continuum Mechanics and Thermodynamics* 1 (1989) 165–196.
- [12] P. Haupt, *Continuum Mechanics and Theory of Materials*, 2nd edition, Springer, 2002.
- [13] D. Helm, Formgedächtnislegierungen, experimentelle Untersuchung, phänomenologische Modellierung und numerische Simulation der thermomechanischen Materialeigenschaften, Universitätsbibliothek Kassel, 2001.
- [14] D. Helm, Stress computation in finite thermoviscoplasticity. *International Journal of Plasticity*, 22 (2006) 1699–1721.
- [15] M. Hockauf, L.W. Meyer, T. Halle, C. Kuprin, M. Hietschold, S. Schulze, L. Krüger, Mechanical properties and microstructural changes of ultrafine-grained AA6063T6 during high-cycle fatigue, *International Journal of Materials Research*, 10 (2006) 1392–1400.

- [16] M. Itskov, On the theory of fourth-order tensors and their applications in computational mechanics, *Computer Methods in Applied Mechanics and Engineering*, 189 (2000) 419–438.
- [17] M. Itskov, The derivative with respect to a tensor: some theoretical aspects and applications, *ZAMM - Journal of Applied Mathematics and Mechanics*, 82, 8 (2002) 535–544.
- [18] M. Itskov, N. Aksel, A closed-form representation for the derivative of non-symmetric tensor power series, *International Journal of Solids and Structures*, 39 (2002) 5963–5978.
- [19] M. Itskov, Computation of the exponential and other isotropic tensor functions and their derivatives, *Computer Methods in Applied Mechanics and Engineering*, 192 (2003) 3985–3999.
- [20] R. F. King, An improved Pegasus method for root finding, *BIT Numerical Mathematics*, 13 (1973) 423–427.
- [21] E. Kröner, Allgemeine Kontinuumstheorie der Versetzungen und Eigenspannungen, *Archive for Rational Mechanics and Analysis*, 4 (1960) 237–334.
- [22] E. H. Lee, Elastic-plastic deformation at finite strains, *Journal of Applied Mechanics*, 91 (1969) 1–6.
- [23] J. Lemaitre, J. L. Chaboche, *Mechanics of solid materials*, University Press, Cambridge, 1990.
- [24] A. Lion, Constitutive modelling in finite thermoviscoplasticity: a physical approach based on nonlinear rheological elements, *International Journal of Plasticity*, 16 (2000) 469–494.
- [25] J. Lu, Exact expansions of arbitrary tensor functions  $\mathbf{F}$  and their derivatives, *International Journal of Solids and Structures*, 41 (2004) 337–349.
- [26] G. Lührs, S. Hartmann, P. Haupt, On the numerical treatment of finite deformations in elastoviscoplasticity, *Computer Methods in Applied Mechanics and Engineering*, 144 (1997) 1–21.
- [27] W. Meyer, F. Hahn, R. Glass, A. Rackova, Werkstoffverhalten und Werkstofffluß bei der partiellen Massivumformung am Beispiel des Bohrungsdrückens, In: *Sächsische Fachtagung Umformtechnik*, 24 (1998) 1–16.
- [28] L.W. Meyer, M. Hockauf, L. Krüger, I. Schneider, Compressive behaviour of ultrafine-grained AA6063T6 over a wide range of strains and strain rates, *International Journal of Materials Research*, (accepted for publication).
- [29] C. Miehe, E. Stein, A canonical model of multiplicative elasto-plasticity: formulation and aspects of the numerical implementation, *European Journal of Mechanics A/Solids*, 11 (1992) 25–43
- [30] C. Miehe, Exponential map algorithm for stress updates in anisotropic multiplicative elastoplasticity for single crystals, *International Journal for Numerical Methods in Engineering*, 39 (1996) 3367–3390.
- [31] F. Mollica, K.R. Rajagopal, A.R. Srinivasa, The inelastic behavior of metals subject to loading reversal, *International Journal of Plasticity*, 17 (2001) 1119–1146.

- [32] P. Perzyna. The constitutive equations for rate sensitive plastic materials, *Quarterly of Applied Mathematics*, 20 (1963) 321–331.
- [33] P. Perzyna, *Fundamental problems in visco-plasticity*, G. Kuerti (Ed.), *Advances in Applied Mechanics*, vol. 9, Academic Press, New York, (1966) 243–377.
- [34] J. H. Poynting, On pressure perpendicular to the shear planes in finite pure shear, and on the lengthening of loaded wires when twisted, *Proceedings of the Royal Society of London. Series A*, 82, 557 (1909) 546–559.
- [35] J. Simo, T. Hughes, *Computational inelasticity*, Springer, 1998.
- [36] J. Simo, C. Miehe, Associative coupled thermoplasticity at finite strains: formulation, numerical analysis and implementation, *Computer Methods in Applied Mechanics and Engineering*, 98 (1992) 41-104.
- [37] B. Svendsen, S. Arndt, D. Klingbeil, R. Sievert, Hyperelastic models for elastoplasticity with nonlinear isotropic and kinematic hardening at large deformation, *International Journal of Solids and Structures*, 35 (1998) 3363-3389.
- [38] Ch. Tsakmakis, Kinematic hardening rules in finite plasticity - Part I: A constitutive approach. Part II: Some examples, *Continuum Mechanics and Thermodynamics*, 8 (1996) 214–246.
- [39] G. Weber, L. Annand, Finite deformation constitutive equations and a time integration procedure for isotropic, hyperelastic-viscoelastic solids, *Computer Methods in Applied Mechanics and Engineering*, 79 (1990) 173–202.
- [40] O. C. Zienkiewicz, R. L. Taylor, *The Finite Element Method, Volume 2: Solid Mechanics*, Butterworth-Heinemann, 2000.